IOPscience iopscience.iop.org

Home Search Collections Journals About Contact us My IOPscience

Rare earth overlayers on silicon

This article has been downloaded from IOPscience. Please scroll down to see the full text article.

1995 J. Phys.: Condens. Matter 7 991

(http://iopscience.iop.org/0953-8984/7/6/006)

View the table of contents for this issue, or go to the journal homepage for more

Download details:
IP Address: 171.66.16.179
The article was downloaded on 13/05/2010 at 11:51

Please note that terms and conditions apply.

J. Phys.: Condens. Matter 7 (1995) 991–1022. Printed in the UK

REVIEW ARTICLE

Rare earth overlayers on silicon

Falko P Netzer
Institut für Experimentalphysik, Karl-Franzens-Universität Graz, A-8010 Graz, Austria

Received 14 September 1994

Abstract. The physiochemical properties of thin layers of rare earth metals and rare earth silicides on Si substrate surfaces are reviewed. The topics discussed include the formation of reactive interfaces at room temperature, the evolution of ordered surface structures at elevated temperature and the oxidation of rare earth interfaces and silicides. Special emphasis is placed on the discussion of the geometrical and electronic structure of ordered overlayer phases.

Contents

1. Introduction
2. Rare earth silicides
3. The formation of reactive interfaces
   3.1. Interfaces at room temperature
   3.2. Temperature evolution of reactive interfaces
4. RE–Si surface superstructures
5. RE silicide overlayers on silicon
   5.1. Epitaxial silicides
   5.2. 2D silicides
6. Oxidation of RE–Si interfaces
7. Conclusions
8. References

1. Introduction

The desire for ever increasing integration in modern semiconductor circuit design led to an intensive search for new contact materials to Si in the late 1970s to early 1980s. It was the pioneering work of Baglin and co-workers [1] at IBM Yorktown Heights that directed the attention of the community to the peculiar properties of rare earth (RE) metal overlayers on Si. They found that thin films of the RE elements Y, Tb and Er react easily with Si(111) and (100) substrates at temperatures as moderate as 300 °C to form silicides of the type $RESi_{2-x}$, with a reaction kinetics that suggested a nucleation controlled formation reaction [2]. Soon afterwards Tu *et al* [3] and Norde *et al* [4] reported that the contacts between RE silicides and Si exhibit unusual Schottky barrier behaviour, with barrier heights of the order of 0.3–0.4 eV for n-Si and 0.7–0.8 eV for p-Si, while Thompson *et al* [5] established that the RE disilicides are good electrical conductors. It was realized that the RE silicides may be classified as a separate class of silicides [6] with distinct and interesting physical

0953-8984/95/060991+32$19.50 © 1995 IOP Publishing Ltd

and chemical properties, amongst them a low temperature of formation, the lowest known Schottky barrier heights on n type Si, a good electrical and thermal conductivity, and an unusual kinetics of formation. Somewhat later it was also recognized that RE silicides may form epitaxially ordered silicide phases on Si(111) [7]. These properties have stimulated fundamental scientific and technological interest in the characterization of RE silicides and of RE overlayers with their interfaces to Si, and this interest seems to have lasted and to continue to date with a tendency to increase over the last half decade. Recent results responsible for this increasing popularity will be presented and emphasized in this review.

Potential device applications of RE silicides in infrared detectors or as ohmic contacts have initially been suggested by Tu *et al* [3] and Norde *et al* [4]; however, two major problems have delayed their practical realization until recently: the stability of the contacts towards environmental influences and the morphology of the silicide thin films. The high oxidation activity of RE elements is well known and RE silicides also react easily with gaseous O_2, yielding ternary phases with physicochemical properties quite different from the original silicides as discussed later in this article. This is an obvious problem for practical application and requires either protecting capping layers or clever device technology as realized only recently [8, 9]. The second problem concerns the stoichiometry and the microstructure of RE silicide films and is connected with material synthesis. Furnace annealing of RE metal overlayers on Si to initiate the silicide reaction yields inhomogeneous films with pits and pinholes as a result of the nucleation controlled formation reaction [1, 10, 11], and these clearly have a detrimental effect on the electrical performance of the structures. Improvements of the thin-film morphologies have been achieved by rapid annealing methods [12–14] and more recently by novel growth techniques involving codeposition of RE metals and Si [15] or intermediate template layers [16–18].

The results on RE–Si interfaces have been reviewed previously by Rossi [19] in a comprehensive treatment, in which the literature up to 1987 has been considered. In view of the above mentioned problems, which hampered the immediate progress in the practical application of RE silicide layers, many of these earlier investigations were devoted to studies of the reactivity at interfaces, in which RE metals were used to model heterogeneous metal–semiconductor interface growth. The chemistry of the RE elements is largely determined by the 5d6s valence electrons and it is therefore typical of low-occupancy d band metals, whereas the 4f electrons act essentially as spectators to the chemistry. However, the latter are useful in the case of a valence change during chemical reactions, where they can provide excellent monitors of the valency. The capability of some RE elements to change their valency as a function of the chemical environment—e.g. Sm, Eu or Yb—has been exploited to advantage to monitor interfacial reactivity, whereby the occupation of the 4f shell, the so-called f count, has been used as a spectroscopic fingerprint in photoemission experiments.

Towards the end of the 1980s high-quality epitaxially grown crystalline RE silicide phases became available, which shifted the emphasis of the scientific interest in these materials and prompted more detailed studies of the electronic and geometrical structures of ordered RE silicide overlayer phases. Also, new two-dimensional (2D) phases of RE silicides in terms of single epitaxial layers have been described [20], with exciting new crystallographic and electronic properties as compared to the material in bulk form. A number of surface reconstructions at submonolayer coverages of RE atoms on Si(111) have been reported recently, and successful attempts to elucidate their structure have been performed [21]. Thin RE metal overlayers have also been tried as catalysts for the low-temperature oxidation of Si. Although it appears that the desired full oxidation to SiO_2 cannot be obtained by this method, new dielectric RE–Si–O phases have been detected and

characterized [22, 23]. All these latter developments will be discussed in some detail in this article, whereas due to space constraints the reactivity at RE–Si interfaces will be treated only briefly.

It is beyond the scope of this treatment to describe the spectroscopic surface sensitive techniques employed in the characterization of the title systems, but a few words on the merits of established techniques and the perspectives of more recently developed methods may be useful in this context. In very crude terms the desired information may be categorized into electronic structure and geometrical structure information, and the techniques may be separated accordingly, with of course some overlap between the two groups. Photoemission techniques in the form of ultraviolet (UV) and x-ray photoelectron spectroscopy (XPS) remain of primary interest for the characterization of the electronic structure of valence and core levels. The use of synchrotron radiation is by now widespread, and the advantages of the tuneable photon energy to enhance the photoemission cross-section of atomic states and thereby the sensitivity for elemental recognition as well as to emphasize the surface sensitivity is generally recognized. Dispersion information on valence bands as obtainable in angle resolved UV photoelectron spectroscopy has become more important recently in this area as a result of the ability to prepare well ordered crystalline phases in epitaxial silicide overlayers. The advent of high-resolution beamlines in synchrotron radiation laboratories in the soft x-ray range is relatively new, but allows us nowadays to extract structure information from XPS spectra by analysing spectral features of atoms, which are located in only slightly different chemical environments on surfaces. Inverse UV photoemission has only recently been applied to RE systems, but it is an important complement to direct photoemission techniques to measure unoccupied electronic states in the conduction band. Auger electron spectroscopy is still largely used as a concentration monitor of surface phases and therefore remains of interest. Apart from diffraction techniques using element specific surface sensitive electron emission from core levels such as photoelectron or Auger electron diffraction, low-energy electron diffraction (LEED) is still generally used to yield important surface structure information, in particular if combined with supplementary information from other electron spectroscopic techniques. As an important new invention the scanning tunnelling microscope (STM) has to be mentioned; this has recently been applied to RE–Si surfaces to give real space insight into the atomic arrangement of ordered RE superstructures on Si or to reveal the morphology of RE silicide thin-film phases. The enumeration of techniques above should not be considered as a comprehensive listing, but rather should give an impression of the more important experimental developments, which will be discussed below.

The review is organized as follows. Section 2 will introduce briefly those properties and aspects of RE silicides of relevance to the main topic of this review. In section 3 I will attempt to give an updated overview of the reactivity at RE–Si interfaces. In section 4 ordered overlayer structures of RE metals will be described and the influence of the valency of the RE atoms on surface reconstructions will be investigated, whereas in section 5 RE silicides in thin-film overlayers will be discussed, with emphasis on epitaxial and 2D phases. Section 6 will present the results of oxidation studies of RE–Si interfaces and RE silicides, and finally some concluding remarks in section 7 will close the article.

2. RE silicides

A major impetus for the study of RE overlayers on Si originated from the technologically motivated need to increase the level of information on the formation processes of RE silicides

on Si substrates. It is therefore appropriate to give a brief introduction into the structural and electronic properties of RE silicides in this section. Thompson and Tu [6] have compared the kinetics of formation, the surface morphology and the electrical properties of RE silicide–Si contacts to those of refractory and noble metals and have concluded that the RE silicides belong to a separate, distinct class amongst the transition metal silicides. The RE silicides occur in three major stoichiometries: in metal rich form as RE_5Si_3 and RE_5Si_4 silicides, as monosilicides RESi and as disilicides of varying composition, $RESi_{2-x}$ with $x \approx 0.25$–0 (from RE_3Si_5 to $RESi_2$). The metal rich silicides crystallize most frequently in the Mn_5Si_3 and Sm_5Ge_4 structures (space groups $P6_3/mcm$ and $Pnma$, respectively) [24], whereas the monosilicides crystallize either in the FeB (space group $Pnma$) or in the CrB ($Cmcm$) structure [25]. However, from the present viewpoint the disilicides are of most interest, since this type of stoichiometry develops upon annealing of RE overlayers on Si [6, 26].

The silicon rich RE compounds of the general formula $RESi_{2-x}$ crystallize in three different structure types, $ThSi_2$, $GdSi_2$, and AlB_2, which are closely related. The type of structure adopted depends on the nature of the RE, on the value of x and on the temperature [27]. With decreasing radius of the RE atom the disilicide is successively tetragonal ($ThSi_2$), orthorhombic ($GdSi_2$) and hexagonal (AlB_2). The tetragonal phase has a composition close to the stoichiometric one ($x = 0$) and the hexagonal phase forms for the RE_3Si_5 stoichiometry ($x = 0.25$), whereas the orthorhombic phase exists for intermedate compositions. The substoichiometric disilicides contain a number of vacancies in the Si sublattice, and the ordering of vacancies leading to superstructures have been reported [28]. The hexagonal lattice of the AlB_2 structure (space group $P6/mmm$) is closely related to the Si lattice and the reported epitaxial growth of the RE disilicides is based on the small lattice mismatch between the two structures for some of the silicides (see section 5).

The electronic structure of RE silicides and the chemical bonding between metal and Si atoms in these compounds have been investigated both experimentally and theoretically. The experimental studies have focused on photoemission techniques probing both the valence region and the core states. As an example figure 1 shows UV photoelectron spectra (UPS) of Gd_5Si_3, GdSi and Gd_3Si_5, thus displaying the occupied valence states, as taken from the work of Braicovich *et al* [29]. The valence band structures are significantly different for the three silicides—note the shift of the structure labelled A in figure 1 in going from Gd_5Si_3 to Gd_3Si_5—and the differences have been associated with a stoichiometry dependent covalent mixing of Gd 5d–Si 3sp states in the formation of the chemical bond [29]. Likewise, the unoccupied conduction band states also display stoichiometry dependence as shown in figure 2, where inverse photoemission spectra (IPES) of Gd_5Si_3 and Gd_3Si_5 are displayed [30].

The Si 2p core levels of RE silicides have been probed by XPS, and the relative Si 2p binding energies of three sets of silicides are collected in table 1. The Si 2p binding energies of the silicides exhibit chemical shifts to lower binding energy with respect to elemental Si, and the shifts increase with increasing metal content of the silicide. The core levels of the metal atoms, however, seem to show only very small chemical shifts in the silicide compounds as compared to the pure metal phases (see e.g. [31, 34–36]). A major goal in carrying out XPS measurements is to obtain information on the chemical state of the atoms in a compound and to interpret chemical shifts of core levels in terms of the charge transfer between the atoms constituting a chemical bond. Unfortunately, however, the effects of the initial state potential change as a result of chemical bond formation and the effects of the change of the relaxation of the spectroscopic final state are intimately mixed and difficult to disentangle. An attempt to obtain a measure of the change in relaxation (screening) energy is to consider the so-called Auger parameter [37]. The Auger parameters of Si in

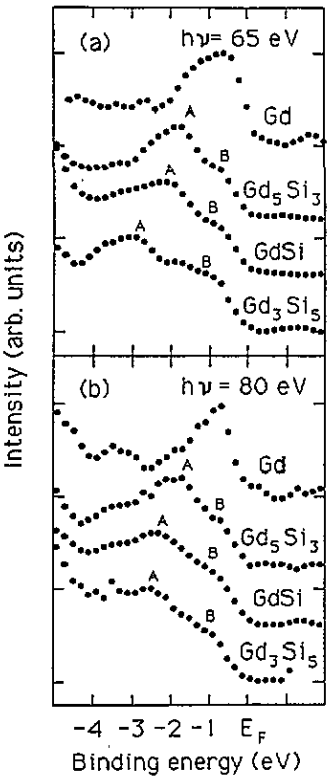

Figure 1. Photoemission spectra of the valence band region of Gd silicides taken at (a) 65 eV and (b) 80 eV photon energy. The upper spectrum in both panels was taken from a metallic sample and is given for reference. (From [29].)

RE silicides appear to be larger than in elemental Si [36, 38], implying a better screening response of the electronic system to the formation of a core hole in the silicides than in Si; this is in accord with the metallic character of the RE silicide compounds. For the case of YSi_{2-x} [38] and $TbSi_{2-x}$ [36] small initial state shifts of the Si 2p core levels and thus weak charge transfer between RE atoms and Si have been derived from a combined analysis of XPS and Auger electron spectroscopy (AES) data.

Table 1. Relative XPS binding energies (eV) of Si 2p core levels of bulk RE silicides, referred to elemental Si as the energy zero.

RE	RE_5Si_3	RESi	RE_3Si_5
Gd [31]	−1.2	−0.7	−0.4
Er [32]	−1.1	−0.7	−0.3
Yb [33]	−1.25	−0.9	−0.5

The chemical bond formation in RE silicides has been discussed following the well established picture of transition metal silicides [39, 40], with particular analogy to the low-d-occupancy metals such as Ca [41] or Sc [40]. Essentially, covalent mixing of RE 5d and Si 3sp states is thought to play the most relevant role for the chemical bond, with the Si 3s states progressively reducing their contribution with increasing metal content of the silicide [42]. The Si 3p derived states are clustered into two regions of bonding (occupied) and antibonding (unoccupied) states below and above the Fermi level [40], while the metal 5d

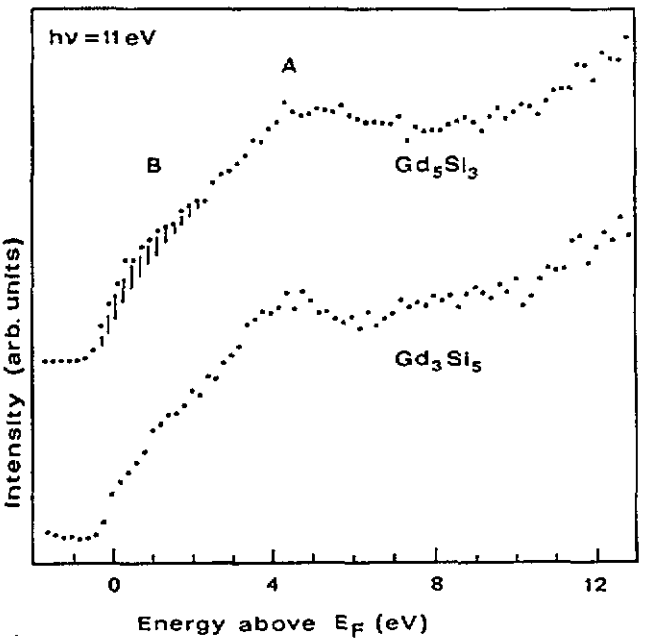

Figure 2. IPES taken at $h\nu = 11$ eV for two Gd silicides. The shaded area represents the difference between the two spectra in the region B, after intensity normalization at feature A. (*From* [30].)

states appear to be concentrated in the region between the bonding and antibonding states around the Fermi level.

Band structure calculations for RE silicides have concentrated thus far on Y and Er disilicides with AlB_2 structure, because these two silicides form epitaxially well ordered phases, which have been characterized extensively by experimental methods [43–47]. The first theoretical study of the electronic structure of YSi_2 by Martinage [43] was performed on the stoichiometric compound and emphasized the importance of the hybridization of the Si p_z and the Y d orbitals as a result of the layer geometry of the system. Augmented plane wave (APW) calculations of the densities of states of YSi_2 and $ErSi_2$ have been compared with experimental XPS and AES results by Magaud *et al* [44], and the discrepancies between theory and experiment have been ascribed to the Si vacancies in the epitaxially grown silicides. The influence of vacancies in the AlB_2 lattice on the band structure of $ErSi_2$ has been addressed explicitly in the extended Hückel calculations of Stauffer *et al* [45]. For both stoichiometric and non-stoichiometric Er disilicide the bands near E_F showed a dominant Er 5d character, but the presence of Si vacancies produced two additional bands in a gap along the ΓA direction, in agreement with experimental observations [45]. Magaud *et al* [46] have performed *ab initio* calculations of the electronic structure of Y disilicide with and without vacancies using the LMTO–ASA method (linear muffin tin orbitals in the atomic sphere approximation) and have shown that the main effect of the vacancies is to stabilize the structure by shifting the Fermi level towards a region of lower density of states at lower energy. Allan *et al* [47] have also investigated the electronic structure of non-stoichiometric Er disilicide with the LMTO method. They concluded that the interaction between the Si and Er valence states is much larger than simple tight-binding estimates would suggest, resulting in a large charge transfer between Er and Si, and suggested that this could be responsible

for the low Schottky barrier at the $ErSi_2$–Si interface. However, as mentioned above, a large charge transfer between RE and Si atoms appears not to be borne out by experimental evidence.

The Yb silicides are particular amongst the RE silicides in that they display mixed valency behaviour [48]. Photoelectron spectra of the 4f emission, taken with synchrotron radiation, have been used to determine the homogeneous mixed valency character of Yb_5Si_3 and YbSi in the bulk, whereas in Yb_3Si_5 inequivalent Yb sites, divalent and mixed valency ones, appear to be occupied [49]. In all compounds the Yb is divalent in the surface region.

3. The formation of reactive interfaces

RE metal overlayers on Si have been considered as prototypical systems to form so-called 'reactive' interfaces. One motivation for the study of RE overlayers on Si surfaces was therefore to model reactive and heterogeneous interface growth. The chemical state dependent valency of some RE elements (e.g. Sm [50,76] or Yb [51]) has been used to advantage to probe multistep interface formation. The major problems addressed in these studies concern the structure of the interface, the nature of the interfacial compound, the electronic states at the interface and the kinetics of the interfacial reaction. Each one of these issues is a complex function of several parameters such as surface orientation, substrate temperature, metal coverage and of course the nature of the deposited metal. Several mechanisms have been proposed to model interface reactions, none of which was able to explain all the experimental observations. A comprehensive general scheme of the major processes that may be involved in interface growth has been presented by Braicovich [52], whereas Butera *et al* [53] and Fujimori *et al* [54] have emphasized thermodynamic aspects to derive a model of reactive metal–semiconductor interface formation.

In a somewhat simplified picture three regimes may be distinguished during the formation of a reactive interface: (i) the weak-interaction regime usually identified with chemisorption; (ii) the intermixing regime where the reaction of the metal with the Si substrate to form silicide-like phases takes place and destroys the Si surface lattice and (iii) the formation of a metal overlayer. In each of these several subregimes and stages may be distinguished [52], depending on the particular system, and several concepts have been proposed for the different stages, such as e.g. the concept of a critical coverage in the transition from (i) to (ii) [52] or the formation of metal clusters as a mechanism to induce the intermixing regime (ii) [52,55]. As far as the RE metals are concerned the general validity of the critical coverage concept is difficult to assess since the data available in the literature are not systematically spread at low coverages. It appears, however, that the chemisorption stage extends up to 0.5–1 monolayer (ML) in most cases, but whether the transition between (i) and (ii) is abrupt or smooth is not always clear. The formation of RE metal clusters at low coverages seems to be the exception rather than the rule: only for Ce [55] and for Tm [56] have metal clusters been proposed. In the following I will separate the discussion according to the substrate temperature, and will first summarize results of interface reactions at room temperature and then of the temperature evolution of interfaces.

3.1. Interfaces at room temperature

The deposition of RE metals onto Si surfaces at room temperature has been mainly investigated by photoelectron spectroscopy techniques, and the use of synchrotron radiation has proved particularly rewarding. A typical example of the evolution of the valence bands as a function of metal coverage is shown in figure 3, where the build-up of a Gd overlayer

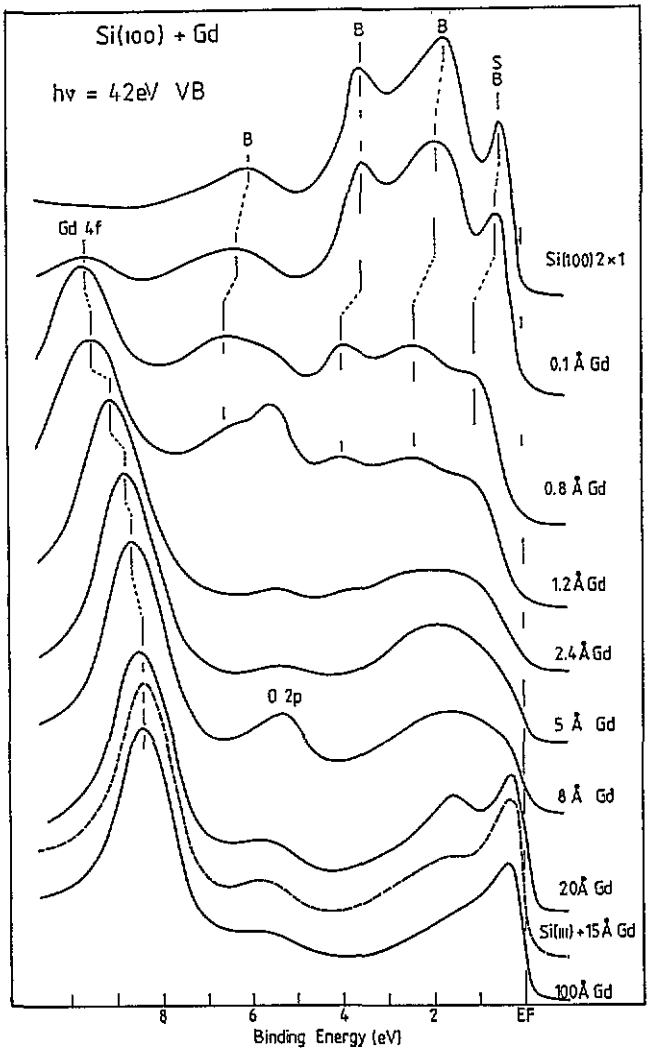

Figure 3. Valence band photoemission spectra of Si(100)2 × 1 as a function of increasing Gd coverage. The spectral curves are normalized arbitrarily to the most intense emission feature. Features B and S are Si bulk and surface derived, respectively. (From [57].)

on Si(100) at room temperature has been followed by UV photoemisison, stimulated with $h\nu = 42$ eV, chosen to ensure high valence band photoemission cross-section as well as high surface sensitivity [57]. During the chemisorption regime up to ~ 1 ML (1 ML = 2.2 Å Gd) the surface states (S) of the clean Si(100)2 × 1 surface are wiped out and the structures due to the bulk valence bands (B) become obliterated. A uniform shift of the whole valence band spectra to higher binding energy (BE) signals a change of the band bending as a result of the Gd surface interaction. Between 1 and 4 ML Gd a broad feature develops around 2 eV binding energy which is characteristic of the intermixing regime, until for ~ 10 ML Gd (~ 20 Å) the well developed valence band structure with peaks at 0.25 eV and 1.6 eV indicates the formation of a well defined interfacial compound. Note that the finite photoemission intensity at the Fermi level demonstrates the metallic character of the

interfacial compound. The metallic Gd film (100 Å) shows the typical triangular valence band shape of the RE metals. The Gd 4f emission moves to lower BE with increasing metal coverage, a behaviour generally observed during the build-up of RE overlayers on Si.

The Si 2p core levels as probed by soft-x-ray photoelectron spectroscopy (SXPS) of the sequence of figure 3 are displayed in figure 4 [57]; the photon energy was 120 eV to ensure high surface sensitivity. The deconvolution of the spectra by standard procedures yields two spin–orbit split Si 2p components of bulk (B) and surface (S) origin for the clean Si(100) surface and accentuates the appearance of a 'reacted' Si 2p component at lower BE (higher kinetic energy, R1 in figure 4), which indicates the onset of the intermixing regime at about $\frac{1}{2}$ ML. For higher Gd coverages a second reacted Si 2p component (R2) at still lower BE is recognized. Analysis of the SXPS data yields the attenuation and growth curves as shown in figure 5, which allow us to identify the various regimes of the interface formation process and which give evidence of a multiphase reacted interface, as has been discussed by Butera *et al* [53].

A compilation of Si 2p core level data of RE–Si interfaces in terms of the chemical shifts of the reacted Si 2p components and of the RE 4f emission is given in table 2. In addition to the reacted Si 2p components R1 and R2 of the room temperature interfaces the relative Si 2p energy positions of the annealed interfaces (see below) and of epitaxial $RESi_{2-x}$ have been included. Both the Si 2p and the RE 4f emissions shift to lower BE as a result of the interaction between RE and Si atoms. However, the shifts of the RE 4f peaks in going from the isolated, adsorbed RE atoms at very low coverages to the metal layer are not solely a straightforward reflection of the RE–Si interaction, but they also include contributions due to ensemble effects as the metal coverages increase. Gokhale *et al* [72] have attempted to interpret the Dy core level shifts with increasing Dy coverage on Si(111) with a charge transfer model: accordingly, the charge transfer from Dy to Si is large for individual adsorbed atoms but decreases at higher metal coverages. However, this charge transfer model neglects the spectroscopic final state effects (relaxation and screening), and represents therefore certainly a too simplistic view.

It can be recognized from table 2 that in most RE–Si systems two reacted Si 2p components may be distinguished during the interface formation process, with chemical shifts of 0.3–0.9 eV for R1 and 1–1.8 eV for R2. Most authors agree that silicide-like phases are formed as interfacial reaction products at room temperature, but the particular stoichiometries are less agreed upon and are in fact less clear. It is likely that at least the R2 phases strive towards a metal rich silicide stoichiometry, as suggested by the comparison of the Si 2p core level energy positions of the R2 components with bulk silicides (see table 1). However, outdiffused Si atoms in an RE metal matrix have also been associated with this large-chemical-shift component [59, 67]. The R1 phase corresponds presumably to an intermediate (monosilicide?) stoichiometry and appears to be inhomogeneous, as suggested by the shift of the corresponding XPS structure with metal coverage (see figure 4) and by the ill defined valence band structure in that coverage regime (see figure 3).

The influence of the Si substrate surface on the interfacial reactivity has been investigated by Rossi *et al* [73] for Yb and by Henle *et al* [57, 64] for Gd. Rossi *et al* have used the mixed valency character of the Yb–Si reaction products as probed by L edge x-ray absorption measurements to gauge the reaction onset and have compared the Yb chemisorption on Si(111)7×7, Si(100)2×1, and ion amorphized Si (a-Si) surfaces [73]. They concluded that the Yb valency is two for monolayer chemisorption on Si(111)7×7, 2.09 on Si(100)2×1 and 2.15 on a-Si, implying an increase of reactivity in that sequence. Similarly, Henle *et al* have studied the interface formation of Gd on Si surfaces by various electron spectroscopies,

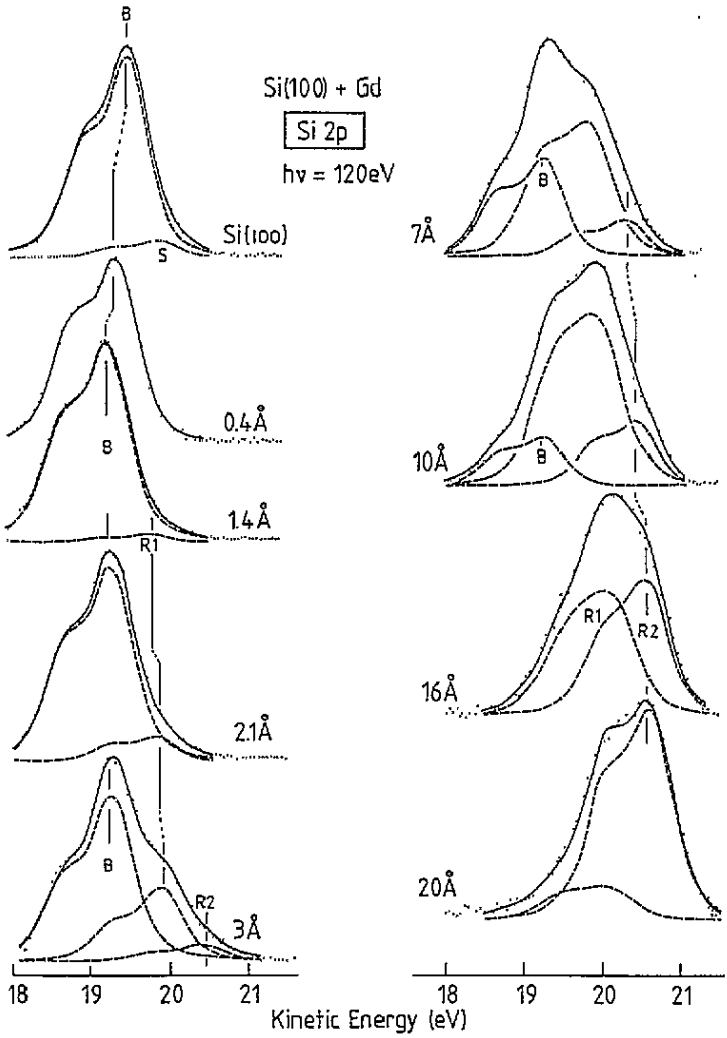

Figure 4. Si 2p core level XPS spectra as a function of Gd coverage. The spectra are normalized to the maximum peak heights, and have been deconvoluted into surface (S), bulk (B) and reacted components (R1 and R2). (From [57].)

observing more pronounced intermixing and a higher rate of reaction for Gd on Si(100)2×1 than on Si(111)7×7 [57].

3.2. The temperature evolution of reactive interfaces

The general pattern of the temperature treatment of reactive RE–Si interfaces may be summarized as a transition from RE metal rich to Si rich silicides upon annealing. Typical results illustrating the change of the total densities of states (DOS) as a result of this transition are shown in figure 6, which presents direct (PES) and inverse photoemission (IPES) spectra of Gd on Si(111) [74]. It is recognized that the DOS emission peak at ~ 1.5 eV below E_F shifts to 2.6 eV, and that the unfilled state peak A above E_F is reduced in intensity in going from the Gd rich to the Si rich (1×1) phase. Comparison with the respective data for

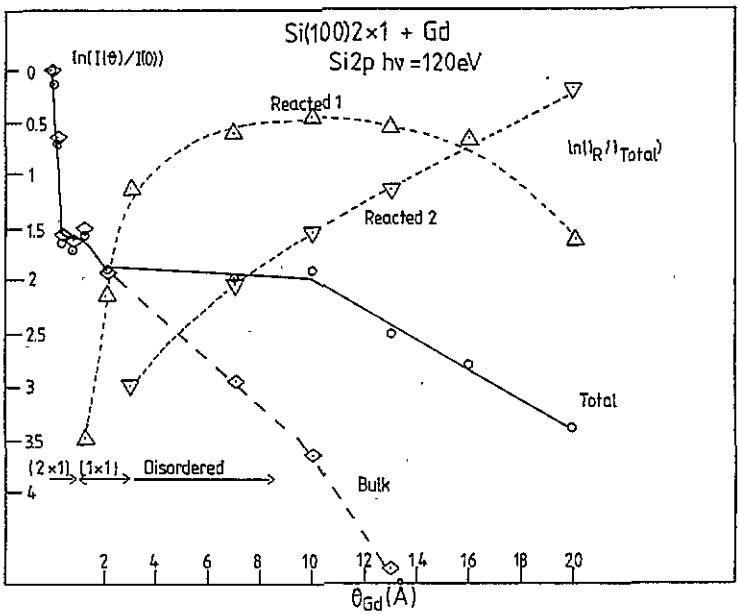

Figure 5. Logarithmic attenuation and growth curves of the Si 2p total, bulk and reacted component photoemission intensities, derived from data as in figure 4, but normalized to constant photon flux. LEED observations are indicated. (From [57].)

Table 2. XPS BE shifts (eV) of Si 2p and RE 4f states at RE–Si interfaces referred to the clean Si surfaces (referenced with respect to the Si 2p bulk component where available) or to RE metal surfaces.

	Si 2p reacted components				RE 4f
	RT[b]		Annealed	Epitaxial	Low
RE[a]	R1	R2	($T \sim 300$–$500\,^{\circ}C$)	$RESi_{2-x}$	coverage
La[a]	−0.35 (0.1)[b]	−1.0 (2) [58]			
Ce/(111)	−0.7(0.6)	−1.2 (> 3) [59]			0.7 (< 0.6) [60]
(100)		−1.3 (5) [61]			
Sm/(111)		−1.2 (~ 8) [50]		−0.4 [21]	
(100)		−1.4 (~ 8) [62]	−0.2 [62]		
Eu	−0.7 (1)	−1.5 (> 2) [63]	−0.7 [63]	−0.4 [63]	0.8 (< 0.2) [63]
Gd/(111)	−0.65 (3) [64]	−1.4 (> 5) [65]		−0.2 [66]	1.25 (< 0.1) [64]
(100)	−0.9 (1)	−1.5 (7) [57]	−0.2 [57]		1.2 (< 0.4) [57]
Tb	−0.85 (~ 1)	−1.15 (5) [34]		−0.1 [36]	1.2 (< 0.4) [34]
Dy	−0.8 (~ 0.5) [67]			−0.4 [67]	
Ho		−1.3 [67]			
Er	−0.7 (1)	−1.3 (6) [32]		−0.3 [32]	~ 1 (0.5) [32]
Tm	−0.3 (2)	−1 (~ 25) [56]	−0.3 [56]	−0.4 [68]	
Yb	−0.9 (1) [69]	−1.8 (8) [70]	−0.5 [69]	−0.3 [69]	
Y		−1.4 (2) [71]		−0.6 [38]	

[a] On Si(111) unless otherwise indicated.

[b] Values in parentheses give the RE coverages in monolayers.

bulk silicides (see figures 1 and 2) confirms the change of the stoichiometry of the interface upon annealing.

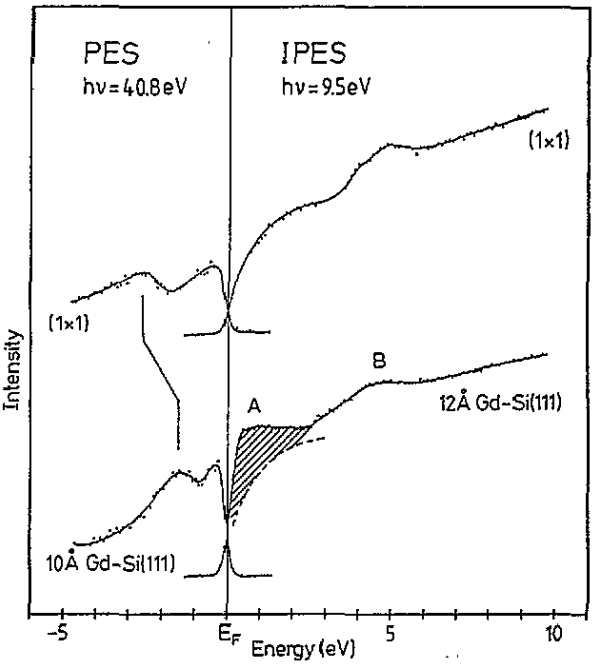

Figure 6. PES and IPES of the reacted room temperature Gd–Si interface and of the (1 × 1) Gd disilicide type phase, which is formed after annealing. The dashed curve and the hatched area in the lower IPES spectrum emphasize the differences in the unfilled DOS between the two phases. (From [74].)

Phase diagrams of RE–Si interfaces describing the temperature behaviour of the interfaces as a function of the RE metal coverage have been established recently for several systems using a combination of AES and LEED [57, 63, 66, 70]. The phase diagram of the Yb–Si(111) interface in the form of a three-dimensional (3D) plot of the Yb Auger signal against temperature as a function of Yb coverage is reproduced in figure 7, from [70]. The diagram illustrates that the Yb content of the interfacial region decreases during gentle annealing for all coverages greater than 1 ML until regions are obtained where ordered phases start to develop for heating temperatures > 250 °C, as indicated by the respective LEED structures. The epitaxial Yb disilicide phases that form for $T \geqslant 300$ °C are characterized by $(\sqrt{3} \times \sqrt{3})R30°$ and (2 × 2) LEED patterns, whereas for $T > 600$ °C ordered Yb–Si surface superstructures are observed as suggested by the low Yb concentration ($\leqslant$ 1 ML) at the surface. These latter surface reconstructions will be discussed further in section 4.

The evolution of the Yb–Si(111) interface with temperature is also illustrated by the SXPS spectra of the Si 2p core levels and of the Yb 4f region for 8 ML Yb–Si(111) as shown in figure 8 [70]. The predominantly divalent Yb of the room temperature interface (Yb rich) becomes of mixed valency after annealing as evidenced by the appearance of Yb^{3+} multiplet features at 6–11 eV binding energy (see the bar diagram in figure 8) and by the shift of the divalent Yb^{2+} features towards E_F; concomitantly the 'reacted' Si 2p emission shifts to higher BE. Of particular interest is the spectroscopic 4f fingerprint of the epitaxial (2 × 2)† Yb disilicide phase at ~ 500 °C: its divalent component is characterized by a single

† The (2 × 2) LEED pattern is actually caused by three equivalent domains of a (2 × 1) surface structure (see [94]).

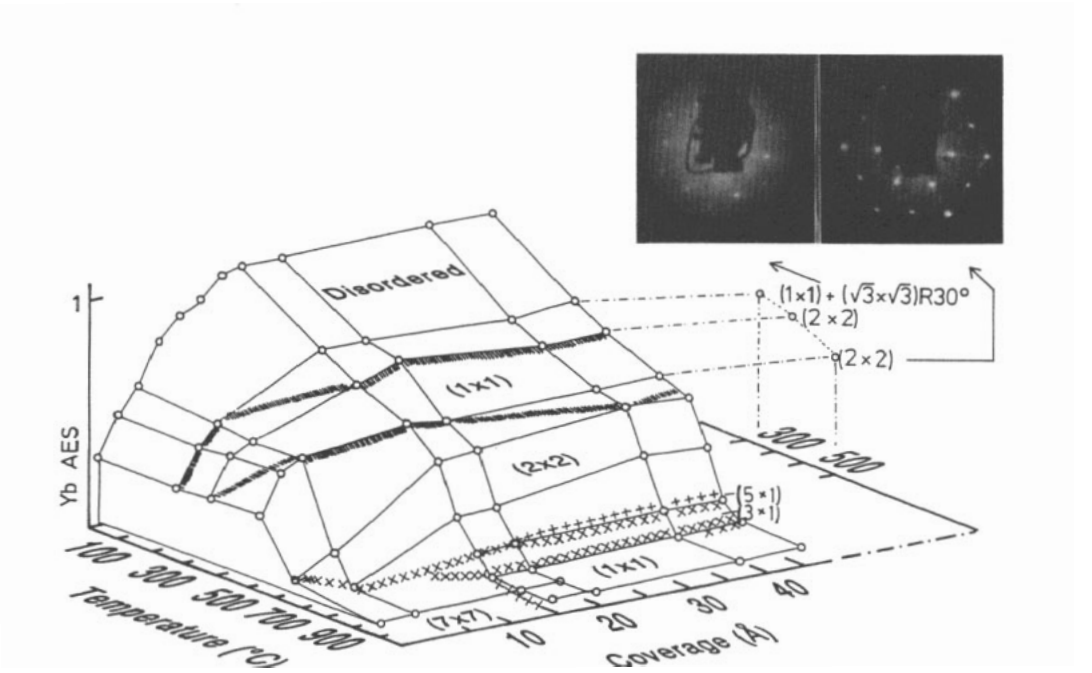

Figure 7. The phase diagram of the Yb–Si(111) interface in the form of a plot of the Yb Auger signal against temperature as a function of Yb coverage (1 ML=3.2 Å). Experimental data points are symbolized by the open circles, and regions of ordered LEED structures are indicated. The data points to the right of the main 3D diagram have been obtained by evaporation of 50 Å Yb onto heated Si substrates. The LEED photographs have been taken from these latter phases. (From [70].)

sharp 4f spin–orbit doublet at E_F, indicating good structural order on the one hand, and the absence of surface 4f components on the other. It has been proposed that the surface of epitaxial $YbSi_{2-x}$ is terminated by a heteroepitaxial Si layer, thus eliminating any surface divalent Yb signal [70]. Note also that the Yb–Si(5 × 1) and (3 × 1) surface reconstructions contain purely divalent Yb atoms.

To summarize briefly, let us stress the following points. After an 'incubation' stage of relatively weak interactions of RE atoms with Si surface atoms of the chemisorptive kind, the destruction of the Si surface lattice and the intermixing of the constituents takes place even at room temperature, followed by interfacial compound formation. In my opinion, no general trend across the RE series in terms of a critical coverage or of the sharpness of the transition between different stages is apparent as yet. The reacted room temperature interfaces are often of multicomponent character, but the most stable interfacial reaction products at room temperature appear to be of the RE rich silicide type. No clear picture has emerged as yet concerning the sharpness of the interfaces, although low temperature seems to yield sharper interfaces as expected [75], nor whether the compound phases are in the form of homogeneous layers or of islands. Si outdiffusion through the metallic RE overlayers has been observed. It is well established that annealing of the reacted room temperature interfaces induces a stoichiometry change from metal rich to Si rich silicides, and that ordered silicide phases are observed in most cases at elevated temperatures.

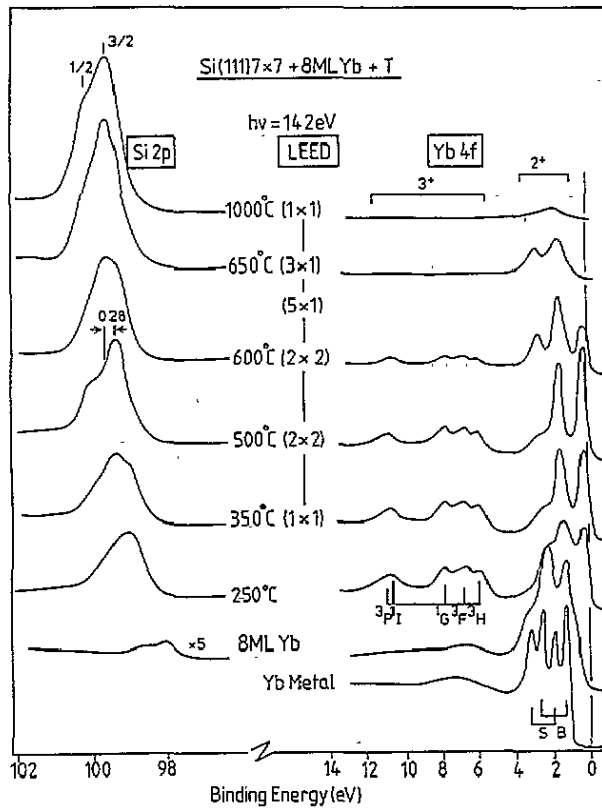

Figure 8. XPS spectra of the Si 2p core levels and of the Yb 4f region for 8 ML Yb on Si(111) and for various phases formed by annealing of the room temperature interface. The bottom curve of the right-hand sequence is from metallic Yb, where surface (S) and bulk (B) divalent 4f components are indicated. The region of divalent and trivalent Yb 4f emission is also designated. (From [70].)

4. RE–Si surface superstructures

In this and the following section various ordered phases of RE–Si overlayer systems will be considered. We begin the discussion with the low-coverage surface superstructures, which are a kind of chemisorbed phase, will continue with conventional thin films of epitaxial RE silicide compounds and will then focus the discussion on the properties of epitaxial 2D RE silicides that form at RE monolayer coverages.

The first observation of ordered surface superstructures on an RE–Si system was reported for Yb–Si(111) by Kofoed *et al* [77]: (2×1), (5×1) and (3×1) LEED patterns were observed after heat treatments of $\leqslant 1$ ML depositions of Yb onto Si(111)7 × 7 surfaces. Since then, other systems have been discovered where RE overlayers in the submonolayer coverage regime induce ordered reconstructions on Si surfaces upon annealing. These systems and the LEED structures observed until mid-1994 are listed in table 3. It is conspicuous that the RE atoms forming the ordered surface superstructures all occur (at least partly) in divalent form. We will discuss this point further below. It is also interesting to note that the RE induced surface superstructures appear to be very stable phases: the structures listed in table 3 can be generated either by annealing of submonolayer to monolayer coverages of

the respective RE metals on Si, or after heating epitaxial RE silicide phases to beyond the decomposition temperature of the disilicide as evident from the phase diagrams of Eu–Si [63] and Yb–Si [70] (see figure 7).

Table 3. LEED structures of RE overlayers at submonolayer to monolayer coverages.

	Increasing RE coverage →	Reference
Si(111):Sm	(3×1) or (3×2), (5×1), (7×1), $(\sqrt{3} \times \sqrt{3})R30°$	[21]
Eu	(3×1), (3×3), (5×5)	[63]
Yb	(3×1) or (3×2), (5×1), (7×1), (2×1)	[70, 78]
Si(100):Sm	(3×2)	[62]

Sm and Yb on Si(111) exhibit several similar metal induced surface structures at low coverages, but show a different reconstruction at higher coverage. Since the Sm valency increases with coverage from two to three, Wigren *et al* [21] have investigated how the difference in valence stability between Sm and Yb influences the type of reconstruction. It is known that trivalent and divalent metals form different surface structures on Si surfaces: compare for example the group III elements, which form $(\sqrt{3} \times \sqrt{3})R30°$ structures at $\frac{1}{3}$ monolayer coverages [79], with the alkaline earth elements on Si [80–82], which display similar $(n \times 1)$ derived structures as listed in table 3. If the saturation of dangling bonds via metal atom bonding is considered to be one of the major driving forces for metal induced surface reconstruction, a trivalent metal atom in a threefold coordinated adsorption site (e.g. T_4 in a $(\sqrt{3} \times \sqrt{3})R30°$ configuration, coverage $\frac{1}{3}$) saturates all dangling bonds on Si(111). Conversely, for a divalent metal atom complete dangling bond elimination on Si(111) is expected at bridge sites in a (2×1) structure at a coverage of $\frac{1}{2}$ ML.

Si 2p spectra from the different Sm and Yb induced surface structures on Si(111) are displayed in figure 9, as taken from the work of Wigren *et al* [21]. The similar core level profiles for the Sm and Yb related structures together with STM observations indicate the same local bonding configuration for both Sm and Yb. From careful inspection of LEED patterns in conjunction with STM imates Wigren *et al* [21] have concluded that the '(3×1)' structure is actually a (3×2) structure, with RE atoms adsorbed in bridge sites. The (3×2) periodicity is also in better agreement, as judged by valence electron counting within the unit cell, with the semiconducting character of the surface than a (3×1) structure. The semiconducting $(n \times 1)$ Sm and Yb structures, which require an even number of valence electrons within the unit cells, are also in disagreement with a simple interpretation of the STM pictures, which show double rows of protrusions at different separations, yielding unit cells with expected odd numbers of electrons. This suggests that the (5×1) and (7×1) structures are quite complicated, involving also reconstructions of the outermost Si(111) layers [21].

The (2×1) structure of Yb has been associated with a surface coverage of $\frac{1}{2}$ ML and bridge site Yb bonding [78], in accord with the above expectation of dangling bond elimination on Si(111) by a divalent metal atom. Whereas Yb is completely divalent in all submonolayer reconstructions, the valency of Sm increases from two to three in going from the (3×2) to the $(\sqrt{3} \times \sqrt{3})R30°$ structure—see figure 10, which shows Sm and Yb 4f spectra from the different surfaces, after Wigren *et al* [21]. The intensity of the trivalent multiplet features in the (5×1) and (7×1) surfaces has been estimated to be $\sim$ 10–20% of the divalent signal, but in the $\sqrt{3}$ structure $\sim$ 50% of the Sm atoms are in the trivalent state (figure 10). As judged by LEED, STM and SXPS the $\sqrt{3}$ Sm structure appears to be a very complex structure consisting of more than one layer, and Wigren *et al* [21] have suggested

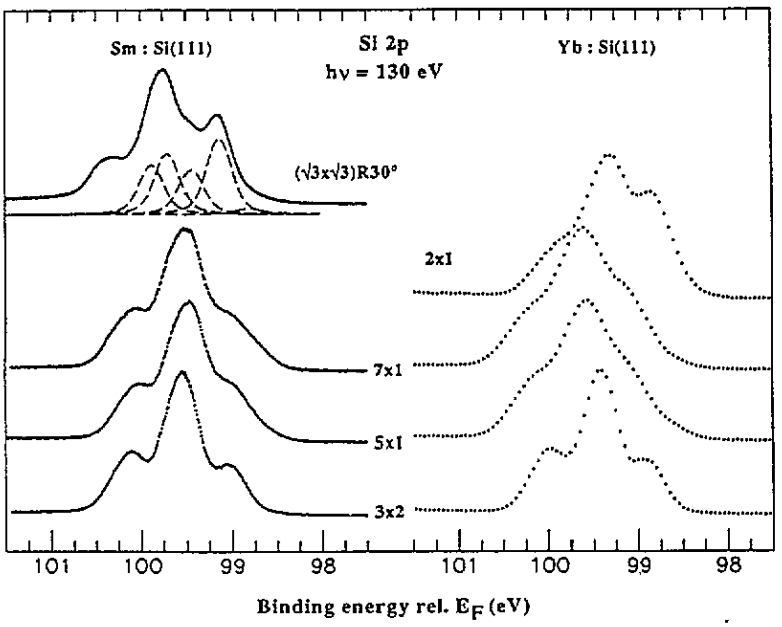

Figure 9. Si 2p spectra from different Sm and Yb induced surface structures on Si(111). The spectrum from the $(\sqrt{3} \times \sqrt{3})R30°$ structure has been fitted with five spin–orbit split components. The full line shows the result of the fit and the dashed lines show the individual $2p_{3/2}$ components. (From [21].)

that a model of this structure should contain trivalent Sm in layers below the surface and divalent Sm in the top layer, the latter in a rather poor long-range order.

However, another train of thought may be developed along the following lines. $\sqrt{3}$ LEED structures are commonly observed on epitaxial $RESi_{2-x}$ phases of trivalent RE elements, and recently a 2D phase of Er silicide consisting of a *single* double layer of $ErSi_2$ has been described [20]. It may be argued that the Sm $\sqrt{3}$ structure is of this 2D silicide type, and support for this conjecture may be obtained from the Fermi level pinning position on this surface. Whereas at the Yb (2×1) surface the Fermi level is fixed close to the middle of the band gap the Sm $\sqrt{3}$ structure has a Fermi level position close to the conduction band minimum [21]. This position is indeed the expected E_F position for a trivalent epitaxial silicide on Si(111) [83]. The following idea may then be generalized: under appropriate annealing conditions the divalent RE elements form true surface superstructures up to 1 ML surface coverage on Si surfaces, whereas the trivalent RE elements tend to develop epitaxial 2D silicide type structures in the region of 1 ML surface coverage. Of course, this suggestion will need additional experiments to test its general validity.

5. RE silicide overlayers on Si

5.1. Epitaxial silicides

The study of the formation of epitaxial RE silicide overlayers constitutes a major area in present day RE–Si research. An important factor in epitaxial growth is the lattice mismatch between the constituents [84]. The $RESi_{1.7}$ compounds crystallize in the AlB_2 structure,

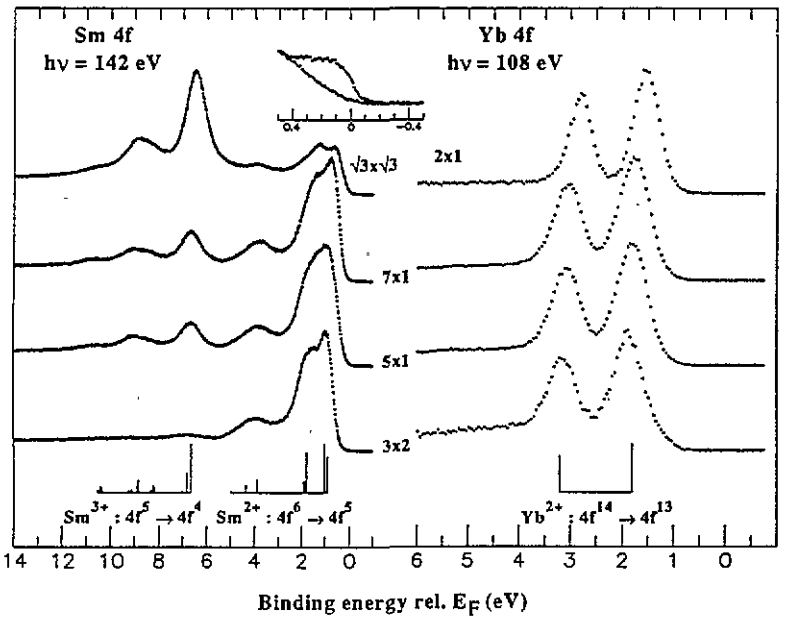

Figure 10. Sm and Yb 4f spectra from different submonolayer metal induced surface reconstructions. Spectra recorded at a photon energy of 40 eV from the Sm induced $(\sqrt{3} \times \sqrt{3})$R30° structure and from a metallic Ta foil are shown in the inset. (From [21].)

where the Si atoms are arranged in a hexagonal plane normal to the silicide *c* axis, which is very similar to that of the (111) surface of Si. This allows interface configurations with lattice mismatches of less than 2%, resulting in nearly perfect epitaxial arrangements. The lattice mismatch to Si(111) has been tabulated by Knapp and Picraux [7] for a number of RE silicides, and the values range from ~ 0% and 0.05% for Y and Tb, respectively, on the low side to −2.0% and −2.55% for Tm and Lu, respectively, on the high side, with the popular Er silicide in between. Therefore, good-quality epitaxial phases of RE silicides are expected to form on Si(111) substrates, and indeed have been reported in the literature [1, 7, 85]. However, conventional furnace annealing of room temperature deposited RE metal films to induce the silicide reaction shows a 'critical temperature' reaction onset behaviour that results in rough, heavily pitted surfaces [10, 11]. This is due to the nucleation phenomena that occur during the RE–Si reaction, instead of atomic diffusion, which controls the formation of most transition metal silicides [86].

Since the Si atoms are the diffusing species in an RE–Si reaction [85], it was suggested earlier [12, 13] that contamination barrier layers at the interface were responsible for the deep pits in the silicide films. However, this seems to be questionable in the light of more recent ultrahigh-vacuum experiments, where clean substrate surfaces have been used. Knapp *et al* [12, 13] have reported that fast electron beam heating, reacting overlayers of RE metals at temperatures of 700–1000 °C for only 200–500 μs, leads to smooth RE silicide surface topologies. The rapid annealing technique has also been used by Hsu *et al* [87], who observed flat and uniform interfaces for laser annealed samples of the light RE elements La, Ce and Nd on Si, while the isothermal furnace annealed interfaces were rough and exhibited a wavelike variation in the location of the interface plane.

Several novel growth techniques have been developed more recently to produce epitaxial

RE silicide films with improved structure and morphology. Arnaud d'Avitaya *et al* [15], for example, have prepared epitaxial Er silicide films on Si(111) by codeposition of Er and Si at a flux ratio close to 1:2 to bypass the nucleation reaction; subsequent annealing up to 900 °C yielded monocrystalline continuous silicide layers. The growth of a thin template layer of silicide followed by codeposition of RE metal and Si and by annealing at 900 °C has been used by Siegal *et al* [16] and Kaatz *et al* [17] to produce uniform Y and Er silicide films with low pinhole densities. Although the investigations of growth techniques have concentrated on the formation Y and Er silicide films, it is expected that similar procedures will be applicable to produce good-quality heteroepitaxial layers of other AlB_2 type silicides. A point of interest in this context is the feasibility of Si re-epitaxy on Er silicide on Si(111), which has been demonstrated by Arnaud d'Avitaya *et al* [15], thus allowing the fabrication of an epitaxial semiconductor–metal–semiconductor heterostructure.

On Si(111) the epitaxial relationship of the hexagonal AlB_2 type silicides is well established with the silicide (0001) plane parallel to the Si(111) plane, but on Si(100) the situation is less straightforward. Nevertheless, epitaxial silicide phases have been reported. Ordered LEED structures have been observed by Henle *et al* [57] after annealing Gd overlayers on Si(100) at 300–400 °C, and Gerőcs *et al* [89] and Molnar *et al* [90] have interpreted their x-ray and electron diffraction measurements on Gd–Si(100) in terms of an epitaxially grown orthorhombic $GdSi_2$ phase, which is rotated by 45° with respect to the Si(100) plane to minimize the lattice mismatch. The epitaxial relationship of Er silicide on Si(100) has been characterized by Lee *et al* [91] using transmission electron microscopy, reflection high-energy electron diffraction and x-ray diffraction: according to these authors the preferred matching face involves the rectangular $(1\bar{1}00)$ side plane of the hexagonal $ErSi_{2-x}$ prism, which fits well along the $\langle 110 \rangle$ directions in Si. Epitaxial growth of $LuSi_{2-x}$ layers has also been reported with better crystallinity on Si(100) than on Si(111) [92].

The first study of the surface crystallography of an RE silicide has been performed on epitaxially grown films of YSi_{2-x} on Si(111) using x-ray photoelectron diffraction [28]. The non-stoichiometric $YSi_{1.7}$ contains an ordered bulk superlattice of Si vacancies that gives a $(\sqrt{3} \times \sqrt{3})R30°$ mesh in the Si surface plane, which is observable by LEED. The top-layer structure of the silicide phase contains a buckled layer of Si atoms with a similar geometry to a (1×1) Si(111) surface [28]. Since $(\sqrt{3} \times \sqrt{3})R30°$ LEED structures are commonly observed on epitaxial phases of the trivalent RE silicides [36, 66, 68, 93], it is expected that this structure of $YSi_{1.7}$ is also characteristic of the surfaces of the other silicides.

The morphology of epitaxial Yb silicide has been investigated by Hofmann *et al* [94] using STM. The STM images demonstrate that the morphology of the silicide films depends critically on the conditions of preparation. Figure 11 shows STM images of epitaxial Yb silicide prepared in two different ways: panel (a) is from 30 Å Yb evaporated onto Si(111)7×7 at room temperature and subsequently annealed to 650 °C, whereas panel (b) has been obtained by evaporating 30 Å Yb onto Si(111)7×7 heated to 500 °C. In the former case large flat islands of Yb silicide of an average size of $\sim 2000 \times 10\,000$ Å and average height of ~ 20 Å are observed, whose top surfaces contain arrays of domain boundaries with hexagonal symmetries, decorated by small spherical particles. The STM picture (a) shows the edge of such an island. In between the island structures large flat areas are discerned where steps of monatomic height and domains of an atomically resolved (2×1) structure can be detected, as also seen by LEED. With the help of scanning tunnelling spectroscopy measurements the spherical particles on top of the islands have been associated with Si clusters and the (2×1) structure has been interpreted as a Yb superstructure on top of the Si substrate [94]. In contrast, evaporation of Yb onto heated Si(111) yields crystallographically well defined '3D' silicide islands with hexagonal, trigonal or rectangular

bases (typical size parameters, 300 Å diameter, 150 Å height) surrounded by a (2×1) Yb–Si layer (figure 11(b)). The pyramidal island shapes suggest that the islands have grown in a layer by layer fashion, and the epitaxial order in this phase is directly manifested in STM images displaying atomic resolution [94]. The overall growth of Yb silicide on Si(111) seems to follow the Stranski–Krastanov mechanism, but the growth kinetics and the resulting island structures are significantly different for the direct silicide reaction during elevated substrate temperature evaporation and for the reaction after formation of a Yb–Si room temperature interface as an intermediate stage.

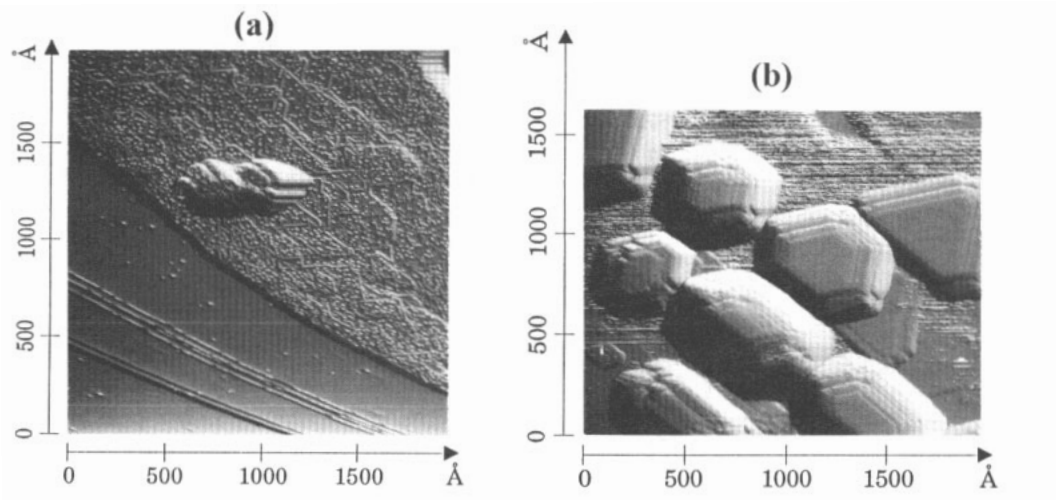

Figure 11. STM images of (a) 30 Å Yb evaporated onto Si(111)7 × 7 at room temperature and heated subsequently to 650 °C and (b) 30 Å Yb evaporated onto Si(111)7 × 7 held at 500 °C. The images were taken with 2 V sample bias and 1 nA tunnelling current. In panel (a) the edge of a large flat Yb silicide island is seen, which rests on a Yb derived (2×1) monolayer type structure, whereas the Yb silicide islands in (b) are more pyramidal shaped with hexagonal, triangular or rectangular bases; they are also surrounded by a (2×1) Yb–Si layer. (From [94].)

The electronic energy band structure in the series of $RESi_{1.7}$ silicides (RE=Y, Gd, Tb, Er) is very similar as demonstrated by the general similarity of the spectral features in angle resolved UV photoemission (ARUPS) spectra. Typical ARUPS profiles of the $GdSi_{1.7}$ $(\sqrt{3} \times \sqrt{3})R30°$ structure are presented in figure 12. The spectra have been recorded with He_I ($h\nu = 21.2$ eV) resonance radiation in the Si $[\bar{1}\bar{1}0]$ azimuth, thus probing states along the $\bar{\Gamma}\bar{K}$ line in the (1×1) surface Brillouin zone [66]. The spectra exhibit a complex behaviour of features as a function of the electron emission angle, but interestingly the general trends in this sequence are quite comparable to those in a similar series of spectra from epitaxial $ErSi_{1.7}$ as published by Wetzel *et al* [95]. From the ARUPS spectra the $\boldsymbol{E}$ against $\boldsymbol{k}$ relation, i.e. the band structure of the solid, can be derived, if suitable assumptions for the final states, e.g. free-electron-like behaviour, are made. Figure 13 shows a comparison between calculated band dispersions and experimental data for $ErSi_{1.7}$ as a function of the perpendicular momentum $k_\perp$ along the ΓA direction, as taken from the work of Stauffer *et al* [45]. There is reasonably good agreement between experimental and theoretical bands with respect to the binding energies as well as to the dispersion of the Si π derived band at 3.7–4.6 eV, the Er d–Si π bands at 2.6–3.1 eV, and the Er d derived bands at 0.2–0.6 eV BE. However, a group of levels located near the A point at $\sim$ 0.9–1.2, 1.8 and 2.2 eV BE

shows poorer agreement with the theoretical bands. These structures have been associated tentatively by Stauffer *et al* with surface state emissions (at 1.8 and 2.2 eV) and with electronic states reflecting the defects of the ordered Si vacancy array (at 0.9–1.2 eV) [45]. The results suggest that the $ErSi_{1.7}$ structure periodicity along the [0001] axis is $2c$ rather than c as a consequence of the ordered arrangement of the Si vacancies.

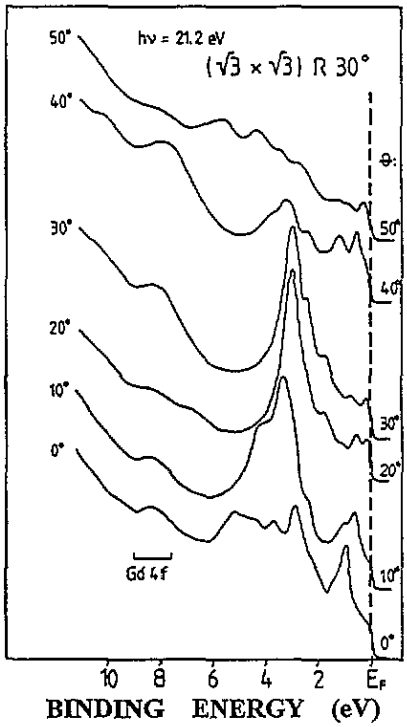

Figure 12. ARUPS of the $(\sqrt{3} \times \sqrt{3})R30°$ $GdSi_{1.7}$ structure. Electrons were detected as a function of the take-off angle Θ, defined with respect to the surface normal, in the $[\bar{1}\bar{1}0]$ crystal azimuth. (From [66].)

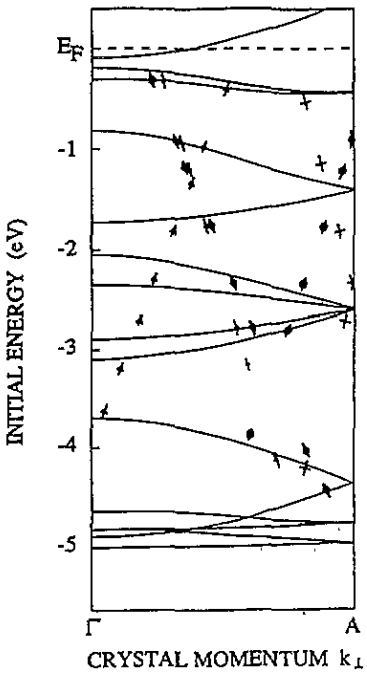

Figure 13. A comparison between calculated (full lines) band dispersions and experimental data for $ErSi_{1.7}$ as a function of the perpendicular momentum $k_\perp$ along the ΓA direction. The calculations are treated by assuming a $2c$ periodicity along the $ErSi_{1.7}$ [001] axis. Data for He_I, He_{II}, Ne_I, Ne_{II} and Ar_I photon energies are shown by the different symbols. (From [45].)

The trivalent RE silicides are metallic as evidenced e.g. by the high DOS at E_F in the UPS spectra (see figure 12), but the divalent RE silicides behave differently and appear to be semi-metallic rather than metallic. This is demonstrated in figure 14, where k resolved IPES of epitaxial Gd $(\sqrt{3} \times \sqrt{3})R30°$ disilicide and Eu (2×2) disilicide are compared. In these experiments the position of the Fermi level E_F has been determined independently from a Ta reference sample [74]. Whereas the trivalent Gd silicide displays significant spectral intensity at E_F, the divalent Eu silicide shows overall a low emission intensity around E_F suggesting a low DOS and thus semimetallic behaviour.

During the last five years considerable progress has been made in the characterization of the electronic and geometrical structure of epitaxial silicide phases of the so-called heavy RE metals, i.e. from Gd to Lu. Much less is known about the silicides of the light RE metals

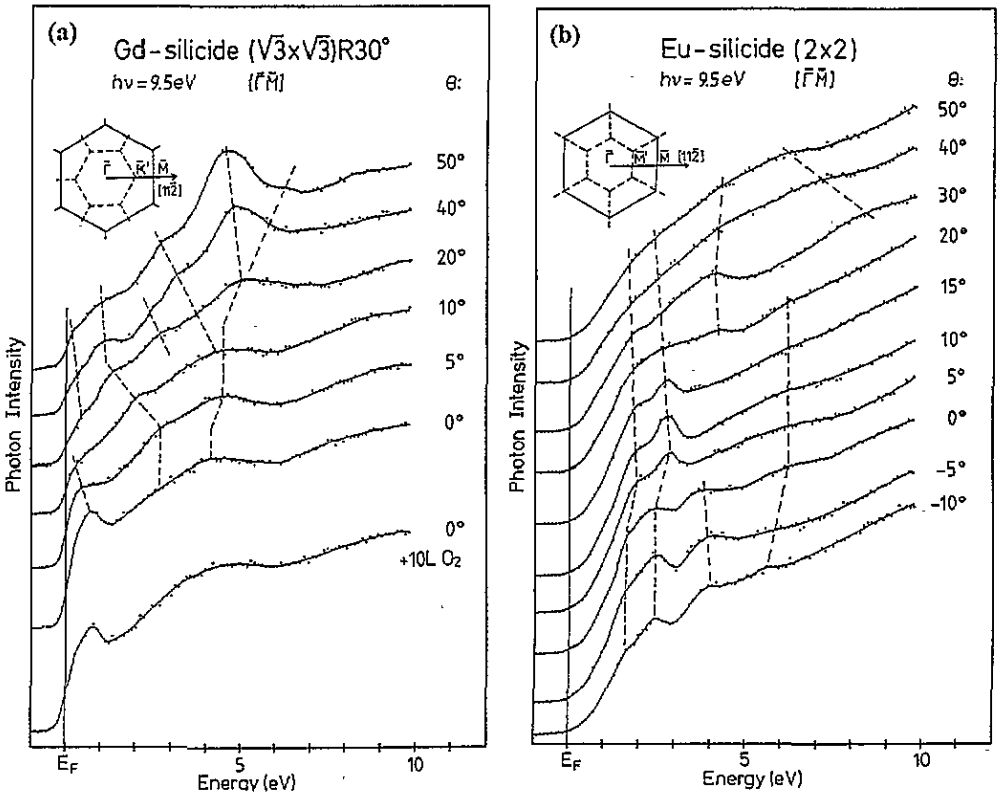

Figure 14. k resolved IPES of (a) the $(\sqrt{3}\times\sqrt{3})$R30° surface of Gd disilicide and (b) the (2×2) surface of Eu disilicide. The insets show the 2D surface Brillouin zones; spectra were measured with $k_{\parallel}$ along the $\bar{\Gamma}\bar{M}$ line. The dashed lines are given as a guide to the eye along possible dispersions. (From [74])

(probably with the exception of Y), and there is ample space for further research in this field. However, a particularly interesting area has been opened up recently by the discovery of 2D quasimonolayer silicide phases, and this will be discussed in the next subsection.

5.2. 2D silicides

Monolayers of Dy, Ho or Er deposited onto Si(111) at room temperature followed by annealing at or above 400 °C convert into epitaxial 2D pseudodisilicide layers with a high degree of crystalline order as evidenced by sharp LEED patterns [67, 20]. In contrast to the bulk phases of epitaxial RE silicides these 2D phases, however, exhibit (1×1) LEED patterns instead of $(\sqrt{3}\times\sqrt{3})$R30° patterns. From photoelectron forward scattering data Paki *et al* [20] have proposed that the Er silicide phase may be viewed as a single epitaxial $ErSi_2$ layer without Si vacancies but with a buckled Si double layer at the top as in bulk Si. The 2D character of this Er disilicide is apparent in figure 15, which presents ARUPS spectra recorded with different photon energies at specific polar angles, so that the component of the photoelectron wave vector parallel to the surface is kept constant near the $\bar{M}$ point of the

surface Brillouin zone (after Wetzel *et al* [96]). Note the very sharp emission peaks located near E_F and at 1.65 eV BE, which display no dispersion with photon energy as required for states having a 2D origin in k space.

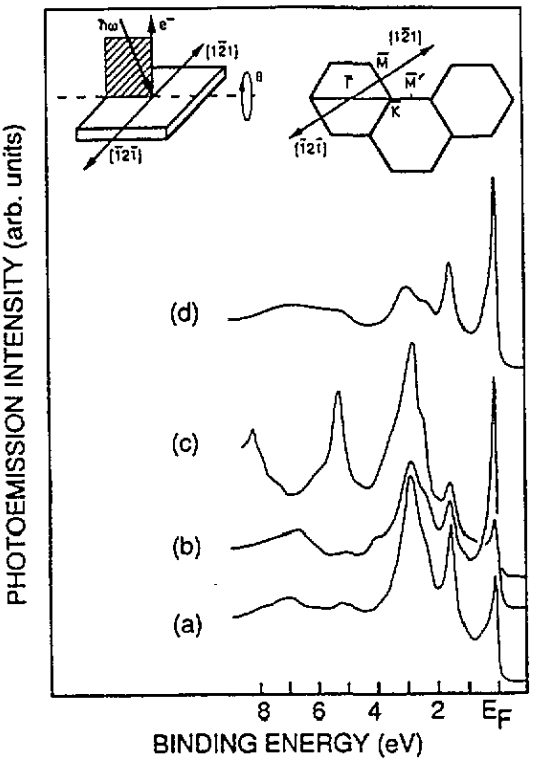

Figure 15. Photoemission spectra taken from the Er surface silicide at point $\bar{M}$ of the surface Brillouin zone (SBZ). They were collected with He_I (a), Ne_I (b) and He_{II} (c) photon energies along the $[1\bar{2}1]$ direction and with He_I (d) photon energy along the $[\bar{1}2\bar{1}]$ direction. Left- and right-hand insets show the experimental geometry and the (1×1) SBZ, respectively. Note that there is no dispersion of features with the same $k_\parallel$ but different $k_\perp$, in agreement with the 2D character of the system. (From [96].)

The band dispersions of the narrow features in the 0–2 eV BE range as obtained from similar ARUPS spectra as in figure 15, but as a function of the electron emission angle θ, have been plotted in figure 16(a): note in particular the periodicity and the extremal behaviour of bands at the equivalent $\bar{M}$ and $\bar{M}'$ points, and the very small portion of a second occupied band at 0.1 eV BE within $k < 0.1$ Å^{-1} around the latter points [96]. Due to its high symmetry and small anisotropy this interesting 2D system allows one to map the Fermi surface quite accurately from a limited set of photoemission data. This has been done in figure 16(b), taken from [96], which shows the measured 2D Fermi surface of the Er surface silicide: it consists of a small hole pocket at $\bar{\Gamma}$ and small electron pockets at $\bar{M}$, which are characteristic of a semi-metal with a small DOS at E_F. In this context Wetzel *et al* have mentioned that this surface silicide should be quite stable as a result of the small band overlap and the low DOS at E_F, and this was indeed what they observed [96].

The experimentally determined bands of the 2D $ErSi_2$ layer have been compared to a theoretical band structure calculated by the crystalline extension of the extended Hückel

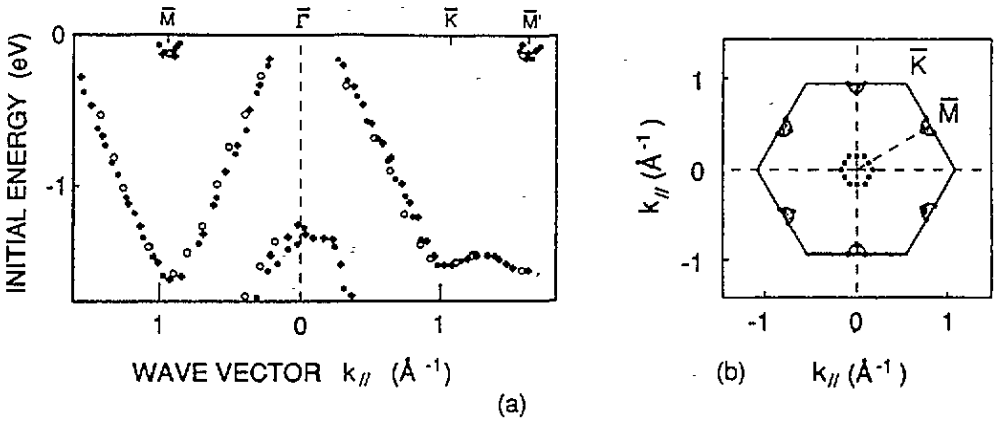

Figure 16. (a) Experimental band dispersions along $\bar{\Gamma}\bar{M}$, $\bar{\Gamma}\bar{K}$ and $\bar{K}\bar{M}'$ symmetry lines for the Er surface silicide. (b) The measured 2D Fermi surface for the Er surface silicide. (From [96].)

method [97]. Using realistic structure models (see below) two characteristic bands near the Fermi level emerged from the calculations that are essentially full and empty and show a topology in agreement with the experiments. Accordingly, the following picture for the chemical bonding in the surface silicide has been proposed by Stauffer *et al* [97]: of the three valence electrons of Er two are involved in the bonding to the Si double layers underneath and above the hexagonal Er layer, whereas the third one is transferred to a large extent to the band of dangling bonds of the topmost Si plane. This should lead to a full occupation of the outwards pointing dangling bonds of the outer Si layer and establish a stable closed shell configuration for all Si atoms. The resulting surface should be inert and in a way akin to the As terminated Si(111) surface. Realistically, however, it is expected that the actual charge transfer to the top layer of Si must be less than one. The upper almost empty band exhibits a strong hybridization between Er 5d and Si 3p states from the Si double layers above and below the Er; it reflects presumably the antibonding character of the Er–Si interaction. It has also been shown that the topology of the calculated bands is particularly sensitive to the relative orientations of the top and substrate Si double layers. Thus, in spite of the weaknesses and quantitative deficiencies of the EHT method a number of possible structure models could be ruled out; moreover, a physical picture of the orbital origin of the surface bands of the 2D silicide has been established [97].

The atomic structure of the 2D $ErSi_2$ has been investigated in the work of Wetzel *et al* [98] using Auger and photoelectron diffraction. The comparison of the Er MNN Auger polar profiles with single-scattering cluster simulations revealed that this silicide phase may be viewed as a single $ErSi_2$ (AlB_2) layer, containing a hexagonal Er monolayer sandwiched between a buckled Si top bilayer and the Si substrate; the top Si bilayer is rotated by 180° around the surface normal relative to the corresponding double layer of the substrate. The buckling of the top layer was found to be comparable to Si(111) and the Er–Si interlayer spacing to be contracted with respect to bulk $ErSi_{1.7}$. Figure 17 illustrates this structure of the Er surface silicide [98]. The interfacial geometry adopted in figure 17 corresponds to the T_4 registry but is tentative, since the scattering geometry employed in the experiments of Wetzel *et al* [98] is insensitive to the interfacial arrangement. However, the calculations of Stauffer *et al* [97] do in fact favour an interfacial geometry with the Er atoms in the threefold-coordinated T_4 hollow sites. Finally it has to be mentioned that only one domain

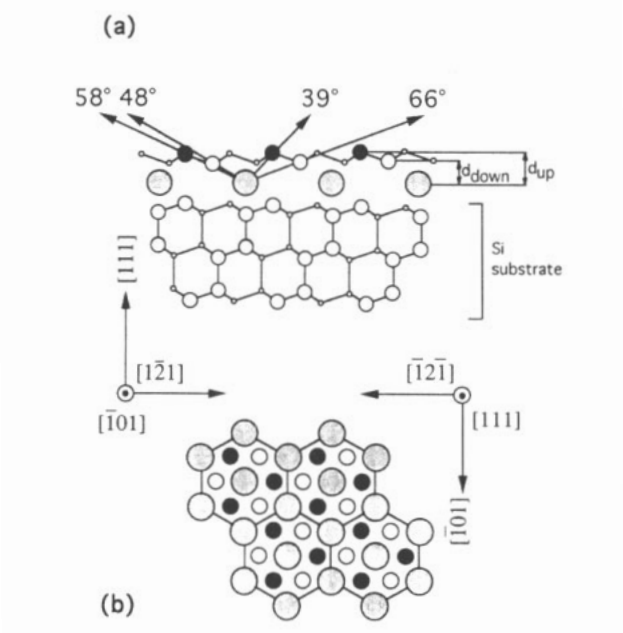

Figure 17. (a) A sketch of the atomic structure of the Er surface silicide projected along the [$\bar{1}$01] direction and (b) a top view of the same structure. Large solid circles denote the Er atoms and small solid circles the Si top-layer atoms. In (a) the large and small open circles represent Si atoms in the plane of the paper and in the ($\bar{1}$01) plane immediately above the paper, respectively. Also indicated are the forward scattering angles expected in the polar profiles of Er MNN Auger emission. The interfacial geometry adopted is tentative and corresponds to the T_4 registry. (From [98].)

of the surface silicide is reportedly formed, and this may be important for device applications since the surface silicide provides a good template layer for Si re-epitaxy.

Up to the time of writing only $ErSi_2$ has been studied in some detail in its 2D form. However, following the report of Sakho *et al* [67] other trivalent RE elements should also form 2D silicides with (1 × 1) LEED structures, and I expect that research activity in this area will increase in the near future.

6. The oxidation of RE–Si interfaces

The interest in the study of the oxidation of RE–Si overlayer systems is motivated by a number of different, but related, aspects. On the one hand, the growth of insulating layers on top of Si is of overwhelming importance in the technology of Si devices, and the search for new dielectric thin-film phases is an essential task in the development of more effective Si based charge coupled devices. On the other hand, since the oxidation of Si to SiO_2, the preferred present day insulator, requires rather severe temperature conditioning, methods to oxidize Si at lower temperatures by means of reactions catalysed by metal overlayers have been investigated extensively. Furthermore, the stability of RE silicide overlayers against environmental influences, e.g. gaseous O_2 or H_2O, is of prime importance for the eventual use of these materials in practical applications. It is therefore appropriate to give a brief account of the oxidation properties of RE–Si systems in this section.

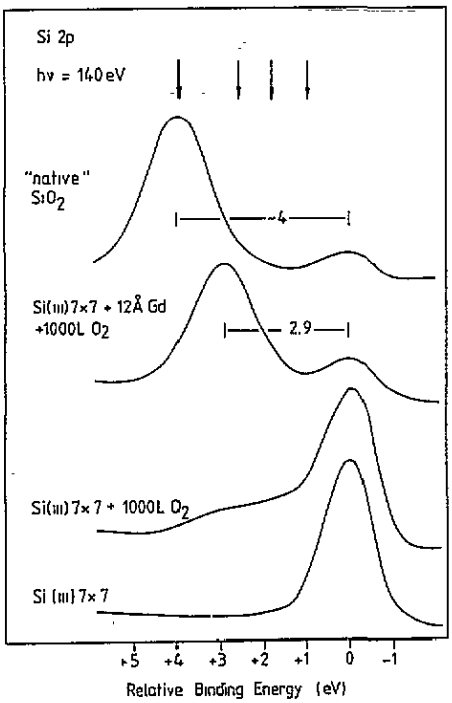

Figure 18. Si 2p core level spectra of Si(111)7 × 7 and of the Si(111)7 × 7 + 12 Å Gd interface exposed to 1000 L O_2 at room temperature. For comparison, a spectrum of the so-called native SiO_2 layer on Si is included (top curve). The arrows indicate Si 2p positions of Si atoms coordinated to one, two, three and four O atoms. (From [22].)

The promotion of the room temperature oxidation of Si by thin metal overlayers has been widely recognized; however, the desired reaction product SiO_2 is rarely obtained in sufficient quality, but instead mixtures of lower Si oxides are often formed. With regard to RE metal overlayers as oxidation catalysts, Hillebrecht *et al* [99] have demonstrated first the enhancement of the oxidation of Si by several orders of magnitude in the presence of a thin overlayer of Ce. Figure 18 illustrates the enhanced oxidation at Si surfaces covered with a thin layer of Gd, in comparison to a clean Si(111)7 × 7 surface, as taken from the more recent work of Henle *et al* [22]. The Si 2p core level spectra of the Si(111)7 × 7 surface show some increased emission intensity at the higher BE side (positive relative BE in figure 18) after exposure to 1000 L O_2† due to oxidized Si atoms, but for the Si(111) surface covered with 12 Å Gd the large, broad peak at ~ +3 eV BE indicates substantial oxidation after the same exposure of 1000 L O_2. The top curve of figure 18 is the Si 2p photoemission spectrum of a 10–15 Å thick layer of SiO_2 on Si(111). The comparison of this latter spectrum with that of the oxidized Gd–Si surface reveals that the two phases are not identical, but that a reaction product different to SiO_2 is formed at the oxidized Gd–Si interface. Apart from the Si the RE metal component of the interface is also oxidized as indicated by XPS on Sm–Si [100] and AES measurements on Gd–Si [101].

Hillebrecht *et al* [99] have suggested that an O deficient Ce pyrosilicate is formed as reaction product at the oxidized Ce–Si interface with a Ce:Si:O composition ratio of 1:1:3.

† 1 Langmuir (L) = 1×10^{-6} Torr s.

Further evidence for ternary silicate type compounds instead of mixtures of binary oxides of Si and RE at oxidized RE–Si interfaces has been obtained more recently by Onsgaard *et al* [100] and Hofmann *et al* [23]. The Si in the pyrosilicates $RE_2Si_2O_7$ is in a formal 4+ oxidation state as in SiO_2 and every Si atom is coordinated to four O atoms; however as a result of the very different structure and bonding in the RE pyrosilicates [102] the Si 2p core level emissions are expected at a different energy position from those of SiO_2. Unfortunately, no XPS reference spectra of RE pyrosilicates are available as yet, but the trend observed here is consistent with that for other silicates [103]. Further evidence for such silicate phases can be inferred from the O KLL Auger spectra [104]. The oxidized RE–Si interfaces yield insulating layers on top of Si with band gaps of the order of 4–6 eV. This has been estimated by Hofmann *et al* [23] by combining PES and IPES, thus probing the total DOS of the structures, as is shown in figure 19. Note that the lower band gap of ~ 4.5 eV of the Eu–Si oxide phase is a result of the localized, filled 4f states of the divalent Eu component of this mixed valency phase.

The enhanced room temperature oxidation of Si in the presence of thin metal overlayers has been discussed in terms of two major promoting effects (see [22] and references therein): (i) reduced activation energy for O_2 dissociation at metal sites and spillover of atomic O to Si and (ii) activation of the Si by disruption of the Si surface lattice as a result of the metal–Si interaction and facile reaction of the activated Si atoms with O. On RE–Si interfaces the rate of oxidation shows a pronounced dependence on the RE coverage, i.e. it is correlated with the number of Si atoms having reacted with RE atoms [22, 23]; this is consistent with the activation of Si by reaction with the RE. On the other hand, evidence has been obtained by AES that the RE constituents of the interfaces are oxidized first, and this suggests that the O_2 dissociates on the RE metal and that the oxidized RE acts as the oxidizing agent [22]. Thus, in the oxidation of RE–Si systems it is difficult to speak of a true catalytic effect of the metal in the classical sense, since the 'catalyst', which should remain chemically unaltered, is also modified by the reaction.

The influence of the valency or of the possibility of a valency change of the RE atoms on the activity of the promoted oxidation of Si has been discussed in the literature [99, 22, 23, 105]. Hofmann *et al* [23] have compared the enhanced room temperature oxidation of Si in the presence of Gd and Eu and have concluded that the valency change from divalent to trivalent, which occurs during the oxidation for Eu, but not for Gd, has no significant influence on the oxidation kinetics. However, in contrast to the high reactivity of the 'reacted', disordered RE–Si room temperature interfaces the epitaxial RE disilicide phases show much less reactivity towards gaseous O_2 [22, 23, 93]. This has been associated with the order and the Si terminated nature of the surfaces of these epitaxial silicides [22]. It should be noted, however, that after an induction period the epitaxial RE disilicides also become oxidized [101].

Finally, I would like to mention an interesting phemonenon that has been observed recently on Eu–Si interfaces: Eu, which remains exclusively divalent during the interaction with pure Si [63], can be switched reversibly between the divalent and the trivalent state by repeated oxidation–reduction cycles effectuated by room temperature O_2 exposure and mild heating of the interface [106, 107]. Since the two valency states of Eu correspond to two magnetically different states (high-spin $^8S_{7/2}$ ground state for Eu^{2+} versus non-magnetic $^7F_0$ for Eu^{3+}), this Eu–Si interfacial structure provides a reversible two-state magnetic system. The valency switching of Eu atoms in a thin layer on Si(111) has been demonstrated by the characteristic 4f fingerprints of Eu^{2+} ($4f^7$) and Eu^{3+} ($4f^6$) in resonant photoemission spectra as shown in figure 20. The divalent Eu of the Eu–Si interface is converted predominantly to the trivalent state by O_2 exposure, and then reverted to divalent by heating the oxidized

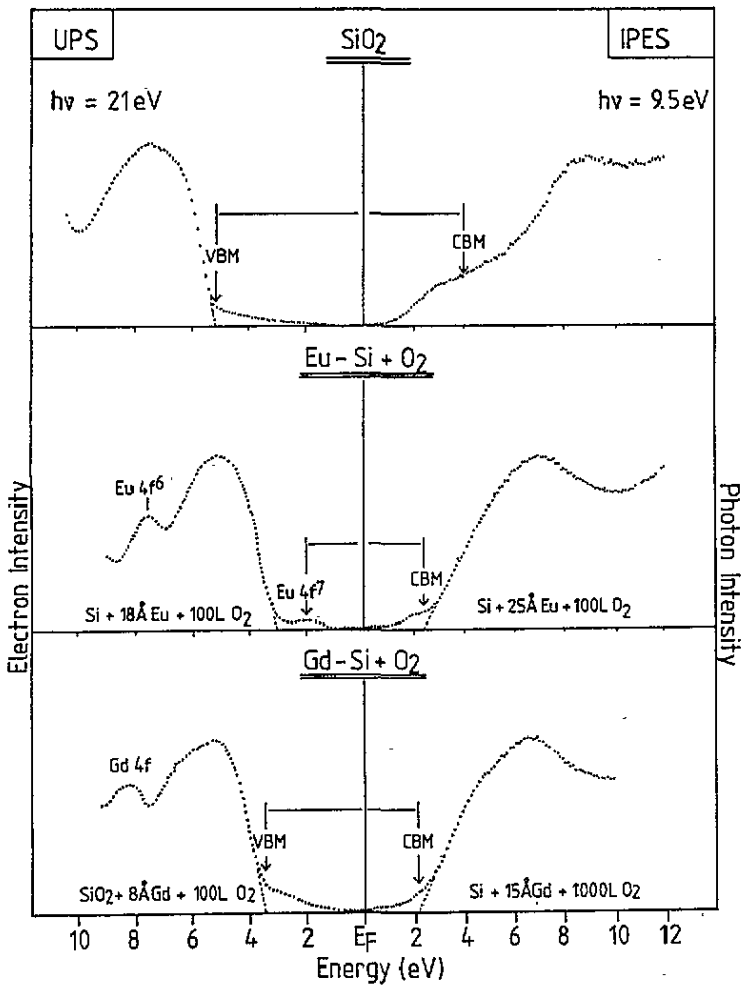

Figure 19. Filled and empty electronic states of SiO_2 and of oxidized Eu–Si and Gd–Si interfaces as seen in UPS and IPES experiments. The band gaps of the different compounds are indicated. (From [23].)

interface to $\sim 200\,^{\circ}C$ for about 30 s. This sequence can be repeated many times, and may also be observed in the $4f^n$–$4f^n$ electron loss structure [107]. It has been proposed that the driving force for the $Eu^{2+} \Leftrightarrow Eu^{3+}$ valency change may be associated with changes in the local O concentration at Eu sites, and that the possibility of reversibility is provided by the Si environment. O_2 exposure increases the local O concentration and induces the divalent to trivalent Eu transition, whereas Si is the reducing agent in the subsequent reversal step, acting as an effective O sink. It has been conjectured that a ternary Eu–Si–O silicate type surface compound with the possibility of Eu in two valences is at the root of this valency switching phenomenon.

7. Conclusions

In the preceding sections of this review I have attempted to highlight various aspects of

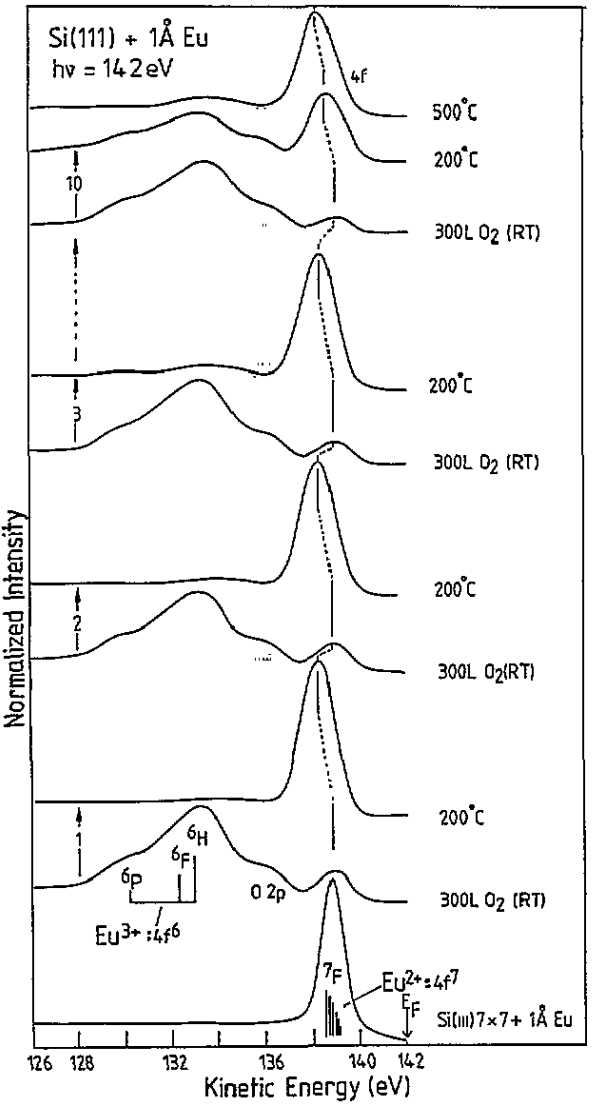

Figure 20. Resonant photoemission spectra of the 4f states of 1 Å Eu–Si(111) during cycles of valency switching between Eu^{2+} and Eu^{3+}, performed by O_2 exposure and subsequent mild heat treatment. The figures on the left-hand side give the numbers of consecutive switches. (From [104].)

the physics and chemistry of overlayers involving RE elements on Si. The processes of formation of interfaces between RE metal overlayers and Si surfaces are now fairly well understood, although the majority of studies has concentrated on (111) oriented surfaces; much less is known about the interfacial reactivity on Si(100) or more complex Si substrate surfaces. High interfacial reactivity between RE metals and Si surfaces at room temperature is generally accepted, and it is also agreed that the interface formation process follows a multistep reaction sequence. In general the resulting room temperature interfaces are inhomogeneous, and metal rich silicide type compounds are mostly encountered as reaction

products. Annealing of the so-called 'reacted' room temperature interfaces converts the metal rich silicide phases to Si rich silicides as interfacial compounds, which are frequently epitaxially ordered. The properties of epitaxial RE silicide overlayers have been discussed in some detail with respect to RE bulk silicides and to recently discovered 2D phases of the disilicides. The observation of ordered surface superstructures of RE atoms on Si(111) in the submonolayer to monolayer coverage range has been reported, and it has been attempted to pick out tentative trends from the limited set of data that are presently available. In a brief section on the oxidation of RE–Si overlayers the formation of ternary RE–Si–O containing compound layers has been mentioned. Due to space limitations of the paper, studies of RE compound overlayers on Si as formed by evaporation from RE compound targets have been omitted from the present discussion. RE oxide and RE fluoride overlayers on Si are amongst the most frequently studied systems investigated in the quest for new dielectric materials on Si—for some representative recent references see [107]–[112].

To round off the article I would like to conclude with a brief outlook on possible future developments. As mentioned before the physicochemical characterization of epitaxial RE silicide overlayers is only at the beginning, and the silicide phases of many more RE elements will have to be tested to obtain a more comprehensive picture of their properties. This is particularly true for the epitaxial 2D phases of RE silicides, which form *extremely well ordered* 2D systems with interesting new possibilities; at present only a flavour of the new phenomena to be expected can be obtained. The RE superstructures on Si may be regarded as prototypical systems for Si surface reconstructions with the participation of *reactive* elements. It will be interesting to contrast the surface structures and trends of the REs with those of the much more investigated surface structures of *non-reactive* metals on Si, such as e.g. the noble metals or the group III metals. Also, the surface chemistry on ordered RE silicide phases may be an active and rewarding area of new research.

In conjunction with the progress in the characterization of fundamental physicochemical properties I expect increased activities in more applied research into RE–Si systems and their incorporation into device technology. The operation of a tunable infrared sensor using a Pt/Si/$ErSi_{1.7}$ heterostructure as an active region has recently been demonstrated [9] and the photoresponse measurements on Er silicide Schottky barrier diodes gave quantum efficiencies comparable to those obtained with Pt silicide diodes, with more to be expected [8]. The study of epitaxial overlayers of Si on thin Er silicide films epitaxially grown on Si(111), the so-called Si re-epitaxy, has now gone beyond the demonstration stage and is entering the phase of detailed spectroscopic characterization [113, 114]. The possibilities of fabricating multilayers of RE silicides and Si and of superlattices have also been pointed out. Thus, it is safe to conclude without too much overoptimism that a bright future of fundamental scientific and technological interest can be foreseen for RE–Si overlayer systems.

Acknowledgments

The undertaking of this review has been made possible by the support of the Austrian Science Foundation. It is my pleasure to acknowledge Professor J A D Matthew, Physics Department, University of York, for many stimulating discussions and for a critical reading of the manuscript.

Note added in proof. Since the completion of the writing of this review Wetzel *et al* 1994 (*Phys. Rev.* B **50** 10866) have suggested, based on ARUPS measurements, that the $(\sqrt{3} \times \sqrt{3})R30°$ bulk phase of epitaxial $ErSi_{1.7}$ is terminated by a buckled Si layer without vacancies, similar to the termination of the corresponding surface silicide. The observed LEED $\sqrt{3}$ superstructure should then reflect the vacancy ordering in the bulk silicide.

References

[1] Baglin J E, d'Heurle F M and Petersson C S 1980 *Appl. Phys. Lett.* **36** 594
[2] Anderson R, Baglin J E, Dempsey J J, Hammer W, d'Heurle F M and Petersson C S 1979 *Appl. Phys. Lett.* **35** 285
[3] Tu K N, Thompson R D and Tsaur B Y 1981 *Appl. Phys. Lett.* **38** 626
[4] Norde H, deSousa Pires J, d'Heurle F M, Pesavento F, Petersson S and Tove P A 1981 *Appl. Phys. Lett.* **38** 865
[5] Thompson R D, Tsaur B Y and Tu K N 1981 *Appl. Phys. Lett.* **38** 535
[6] Thompson R D and Tu K N 1982 *Thin Solid Films* **93** 265
[7] Knapp J A and Picraux S T 1986 *Appl. Phys. Lett.* **48** 466
[8] Unewisse M H and Storey J W V 1992 *J. Appl. Phys.* **72** 2367
[9] Pahun L, Campidelli Y, Arnaud d'Avitaya F and Badoz P A 1992 *Appl. Phys. Lett.* **60** 1166
[10] Lau S S, Pai C S, Wu C S, Kuech T F and Liu B X 1982 *Appl. Phys. Lett.* **41** 77
[11] Wu C S, Lau S S, Kuech T F and Liu B X 1983 *Thin Solid Films* **104** 175
[12] Knapp J A, Picraux S T, Wu C S and Lau S S 1984 *Appl. Phys. Lett.* **44** 747
[13] Knapp J A, Picraux S T, Wu C S and Lau S S 1985 *J. Appl. Phys.* **58** 3747
[14] Youn C, Jungling K and Grannemann W W 1988 *J. Vac. Sci. Technol.* A **6** 2474
[15] Arnaud d'Avitaya F, Perio A, Oberlin J-C, Campidelli Y and Chroboczek J A 1989 *Appl. Phys. Lett.* **54** 2198
[16] Siegal M P, Kaatz F H, Graham W R, Santiago J J and Van der Spiegel J 1989 *Appl. Surf. Sci.* **38** 162
[17] Kaatz F H, Graham W R and Van der Spiegel J 1993 *Appl. Phys. Lett.* **62** 1748
[18] Duboz J-Y, Badoz P-A, Perio A, Oberlin J-C, Arnaud d'Avitaya F, Campidelli Y and Chroboczek J A 1989 *Appl. Surf. Sci.* **38** 171
[19] Rossi G 1987 *Surf. Sci. Rep.* **7** 1
[20] Paki P, Kafader U, Wetzel P, Pirri C, Peruchetti J C, Bolmont D and Gewinner G 1992 *Phys. Rev.* B **45** 8490
[21] Wigren C, Andersen J N, Nyholm R, Göthelid M, Hammar M, Törnevik C and Karlsson U O 1993 *Phys. Rev.* B **48** 11 014
[22] Henle W A, Ramsey M G, Netzer F P, Cimino R, Braun W and Witzel S 1990 *Phys. Rev.* B **42** 11 073
[23] Hofmann R, Henle W A and Netzer F P 1991 *Phys. Rev.* B **44** 3133
[24] Samsonov G B, Drovina L A and Rud B M 1979 *Silicides* (Moscow: Metallurgija)
[25] Hohnke D and Parthé E 1966 *Acta Crystallogr.* **20** 572
[26] Koleshko V M, Belitsky V F and Khodin A A 1986 *Thin Solid Films* **141** 277
[27] Houssay E, Rouault A, Thomas O, Madar R and Senateur J P 1989 *Appl. Surf. Sci.* **38** 156
[28] Baptist R, Ferrer S, Grenet G and Poon H C 1990 *Phys. Rev. Lett.* **64** 311
[29] Braicovich L, Puppin E, Lindau I, Iandelli A, Olcese G L and Palenzona A 1990 *Phys. Rev.* B **41** 3123
[30] Chemelli C, Luridiana S, Sancrotti M, Braicovich L, Ciccacci F, Iandelli A, Olcese G L and Palenzona A 1990 *Phys. Rev.* B **42** 1829
[31] Puppin E, Lindau I and Abbati I 1991 *Solid State Commun.* **77** 983
[32] Wetzel P, Haderbache L, Pirri C, Peruchetti J C, Bolmont D and Gewinner G 1991 *Phys. Rev.* B **43** 6620
[33] Abbati I, Braicovich L, Carbone C, Nogami J, Lindau I, Iandelli I, Olcese G and Palenzona A 1987 *Solid State Commun.* **62** 35
[34] Kennou S, Veuillen J-Y and Nguyen Tan T A 1992 *Appl. Surf. Sci.* **56–58** 520
[35] Veuillen J-Y, Nguyen Tan T A, Lollman D B B, Cinti R and Guerfi N 1991 *Surf. Sci.* **251/252** 432
[36] Veuillen J-Y, Kennou S and Nguyen Tan T A 1991 *Solid State Commun.* **79** 795
[37] Wagner C D and Joshi A 1988 *J. Electron Spectrosc. Relat. Phenom.* **47** 283
[38] Baptist R, Pellissier A and Chauvet G 1988 *Solid State Commun.* **68** 555
[39] Calandra C, Bisi O and Ottaviani G 1984 *Surf. Sci. Rep.* **4** 271
[40] Weaver J H, Franciosi A and Moruzzi V L 1984 *Phys. Rev.* B **29** 3293
[41] Bisi O, Braicovich L, Carbone C, Lindau I, Iandelli A, Olcese G L and Palenzona A 1989 *Phys. Rev.* B **40** 10 194
[42] Sancrotti M, Iandelli A, Olcese G L and Palenzona A 1991 *Phys. Rev.* B **44** 3328
[43] Martinage L 1989 *J. Phys.: Condens. Matter* **1** 2593
[44] Magaud L, Veuillen J Y, Lollman D, Nguyen Tan T A, Papaconstantopoulos D A and Mehl M J 1992 *Phys. Rev.* B **46** 1299
[45] Stauffer L, Pirri C, Wetzel P, Mharchi A, Paki P, Bolmont D, Gewinner G and Minot C 1992 *Phys. Rev.* B **46** 13 201
[46] Magaud L, Julien J P and Cyrot-Lackmann F 1992 *J. Phys.: Condens. Matter* **4** 5399

[47] Allan G, Lefebvre I and Christensen N E 1993 *Phys. Rev.* B **48** 8572
[48] Abbati I, Braicovich L, Del Pennino U, Iandelli A, Olcese G L, Palenzona A, Carbone C, Nogami J, Yeh J J and Lindau I 1985 *Physica* B **130** 141
[49] Abbati I, Braicovich L, Carbone C, Nogami J, Lindau I, Iandelli I, Olcese G and Palenzona A 1987 *Solid State Commun.* **62** 35
[50] Franciosi A, Weaver J H, Perfetti P, Katnani A D and Margaritondo G 1983 *Solid State Commun.* **47** 427
[51] Rossi G, Nogami J, Yeh J J and Lindau I 1983 *J. Vac. Sci. Technol.* B **1** 530
[52] Braicovich L 1988 *The Chemical Physics of Solid Surfaces and Heterogeneous Catalysis* vol 5, ed D A King and D P Woodruff (Amsterdam: Elsevier) p 235
[53] Butera R A, del Giudice M and Weaver J H 1986 *Phys. Rev.* B **33** 5435
[54] Fujimori A, Grioni M and Weaver J H 1986 *Phys. Rev.* B **33** 726
[55] Grioni M, Joyce J, Chambers S A, O'Neill D G, del Giudice M and Weaver J H 1984 *Phys. Rev. Lett.* **53** 2331
[56] Gokhale S, Mahamuni S, Joshi K, Nigavekar A S and Kulkarni S K 1991 *Surf. Sci.* **257** 157
[57] Henle W A, Ramsey M G, Netzer F P, Witzel S and Braun W 1991 *Surf. Sci.* **243** 141
[58] Puppin E, Guyot H, Shen Z X, Hwang J and Lindau I 1988 *Solid State Commun.* **67** 23
[59] Grioni M, Joyce J, del Giudice M, O'Neill D G and Weaver J H 1984 *Phys. Rev.* B **30** 7370
[60] Grioni M, Joyce J, Chambers S A, O'Neill D G, del Giudice M and Weaver J H 1984 *Phys. Rev. Lett.* **53** 2331
[61] Hillebrecht F U 1989 *Appl. Phys. Lett.* **55** 277
[62] Onsgaard J, Ghijsen J, Johnson R L, Ørskov F, Chorkendorff I and Grey F 1990 *J. Electron Spectrosc. Relat. Phenom.* **52** 67
[63] Henle W A, Ramsey M G, Netzer F P and Horn K 1991 *Surf. Sci.* **254** 182
[64] Henle W A, Netzer F P, Cimino R and Braun W 1989 *Surf. Sci.* **221** 131
[65] Henle W A 1990 *PhD Thesis* University of Innsbruck
[66] Henle W A, Ramsey M G, Netzer F P, Cimino R and Braun W 1989 *Solid State Commun.* **71** 657
[67] Sakho O, Sirotti F, DeSantis M, Sacchi M and Rossi G 1992 *Appl. Surf. Sci.* **56–58** 568
[68] Wigren C, Andersen J N, Nyholm R and Karlsson U O 1993 *J. Vac. Sci. Technol.* A **11** 2665
[69] Braicovich L, Abbati I, Carbone C, Nogami J and Lindau I 1986 *Surf. Sci.* **168** 193
[70] Hofmann R, Henle W A, Netzer F P and Neuber M 1992 *Phys. Rev.* B **46** 3857
[71] Pellissier A, Baptist R and Chauvet G 1989 *Surf. Sci.* **210** 99
[72] Gokhale S, Ahmed N, Mahamuni S, Rao V J, Nigavekar A S and Kulkarni S K 1989 *Surf. Sci.* **210** 85
[73] Rossi G, Chandesris D, Roubin P and Lecante J 1986 *Phys. Rev.* B **33** 2926
[74] Hofmann R and Netzer F P 1991 *Phys. Rev.* B **43** 9720
[75] Puppin E and Lindau I 1989 *Solid State Commun.* **71** 1015
[76] Sakho O, Sacchi M, Sirotti F and Rossi G 1993 *Phys. Rev.* B **47** 3797
[77] Kofoed J, Chorkendorff I and Onsgaard J 1984 *Solid State Commun.* **52** 283
[78] Wigren C, Andersen J N, Nyholm R, Karlsson U O, Nogami J, Baski A A and Quate C F 1993 *Phys. Rev.* B **47** 9663
[79] Uhrberg R I G and Hansson G V 1991 *Crit. Rev. Solid State Mater. Sci.* **17** 133
[80] Quinn J and Jona F 1991 *Surf. Sci. Lett.* **249** L307
[81] Fan W C, Wu N J and Ignatiev A 1990 *Phys. Rev.* B **42** 1254
[82] Olmstead M A, Uhrberg R I G, Bringans R D and Bachrach R Z 1986 *J. Vac. Sci. Technol.* B **4** 1123
[83] Duboz J Y, Badoz P A, Arnaud d'Avitaya F and Chroboczek J A 1989 *Appl. Phys. Lett.* **55** 84
[84] Zur A, McGill T C and Nicolet M-A 1985 *J. Appl. Phys.* **57** 600
[85] Baglin J E E, d'Heurle F M and Petersson C S 1981 *J. Appl. Phys.* **52** 2841
[86] Petersson S, Anderson R, Baglin J, Dempsey J, Hammer W, d'Heurle F and LaPlaca S 1980 *J. Appl. Phys.* **51** 373
[87] Hsu C C, Wang Y X, Hu J, Ho J and Qian J J 1989 *J. Vac. Sci. Technol.* A **7** 3016
[88] Siegal M P, Kaatz F H, Graham W R, Santiago J J and Van der Spiegel J 1989 *Appl. Surf. Sci.* **38** 162
[89] Gerőcs I, Molnar G, Jaroli E, Zsoldos G, Petö G, Gyulai J and Bugiel E 1987 *Appl. Phys. Lett.* **51** 2144
[90] Molnar G, Petö G and Zsoldos E 1993 *Appl. Surf. Sci.* **70/71** 466
[91] Lee Y K, Fujimura N, Ito T and Itoh N 1993 *J. Cryst. Growth* **134** 247
[92] Travlos A, Aloupogiannis P, Rokofyllou E, Papastaikoudis C, Weber G and Traverse A 1992 *J. Appl Phys.* **72** 948
[93] Veuillen J-Y, Magaud L, Lollman D B B and Nguyen Tan T A 1992 *Surf. Sci.* **269/270** 964
[94] Hofmann R, Netzer F P, Patchett A J, Barrett S D and Leibsle F M 1993 *Surf. Sci.* **291** 402
[95] Wetzel P, Haderbache L, Pirri C, Peruchetti J C, Bolmont D and Gewinner G 1991 *Surf. Sci.* **251/252** 799
[96] Wetzel P, Pirri C, Paki P, Peruchetti J C, Bolmont D and Gewinner G 1992 *Solid State Commun.* **82** 235

[97] Stauffer L, Mharchi A, Pirri C, Wetzel P, Bolmont D, Gewinner G and Minot C 1993 *Phys. Rev.* B **47** 10 555
[98] Wetzel P, Pirri C, Paki P, Bolmont D and Gewinner G 1993 *Phys. Rev.* B **47** 3677
[99] Hillebrecht F U, Ronay M, Rieger D and Himpsel F J 1986 *Phys. Rev.* B **34** 5377
[100] Onsgaard J, Ghijsen J, Johnson R L, Christiansen M, Ørskov F and Godowski P J 1991 *Phys. Rev.* B **43** 4216
[101] Henle W A, Ramsey M G and Netzer F P 1990 *Vacuum* **41** 814
[102] Smolin Y I and Shepelev Y F 1970 *Acta Crystallogr.* B **26** 484
[103] Briggs D and Seah M P (ed) 1990 *Practical Surface Analysis* 2nd edn, vol 1 (Chichester: Wiley) appendix 5
[104] Öfner H, Netzer F P and Matthew J A D 1992 *J. Phys.: Condens. Matter* **4** 9795
[105] Chang S, Philip P, Wall A, Raisanen A, Troullier N and Franciosi A 1987 *Phys. Rev.* B **35** 3013
[106] Henle W A, Ramsey M G, Netzer F P and Horn K 1991 *Appl. Phys. Lett.* **58** 1605
[107] Matthew J A D, Hofmann R, Öfner H and Netzer F P 1992 *J. Phys.: Condens. Matter* **4** 8489
[108] Inoue T, Yamamoto Y, Koyama S, Suzuki S and Ueda Y 1990 *Appl. Phys. Lett.* **56** 1332
[109] Inoue T, Ohsuna T, Luo L, Wu X D, Maggiore C J, Yamamoto Y, Sakurai Y and Chang J H 1991 *Appl. Phys. Lett.* **59** 3604
[110] Cranton W M, Spink D M, Stevens R and Thomas C B 1993 *Thin Solid Films* **226** 156
[111] McMullin P G and Sinharoy S 1988 *J. Vac. Sci. Technol.* A **6** 1367
[112] Colbow K M, Gao Y, Tiedje T, Dahn J R, Reimers J N and Cramm S 1992 *J. Vac. Sci. Technol.* A **10** 765
[113] Nguyen Tan T A, Veuillen J-Y, Kennou S and Magaud L 1993 *Appl. Surf. Sci.* **70/71** 520
[114] Veuillen J-Y, d'Anterroches C and Nguyen Tan T A 1994 *J. Appl. Phys.* **75** 223